Reprogramming astrocytic NDRG2/NF-κB/C3 signaling restores the diabetes-associated cognitive dysfunction

Tao Jiang,[a,b,e] Yansong Li,[a,e] Shuxuan He,[a] Ning Huang,[a,c,d] Mengyu Du,[a] Qian Zhai,[a] Kairui Pu,[a] Meiyan Wu,[a] Chaoying Yan,[a] Zhi Ma,[a] and Qiang Wang[a,*]

[a]Department of Anesthesiology & Center for Brain Science, The First Affiliated Hospital of Xi'an Jiaotong University, Xi'an 710061, Shaanxi, China
[b]Department of Anesthesiology, The Second Affiliated Hospital of Xi'an Jiaotong University, Xi'an 710004, Shaanxi, China
[c]Department of Physiology and Pathophysiology, School of Basic Medical Sciences, Xi'an Jiaotong University Health Science Center, Xi'an 710061, Shaanxi, China
[d]Institute of Neuroscience, Translational Medicine Institute, Xi'an Jiaotong University Health Science Center, Xi'an 710061, Shaanxi, China

eBioMedicine
2023;93: 104653
Published Online xxx
https://doi.org/10.1016/j.ebiom.2023.104653

Summary

Background Dementia is a serious complication in patients with diabetes-associated cognitive dysfunction (DACD). In this study, we aim to explore the protective effect of exercise on DACD in diabetic mice, and the role of NDRG2 as a potential guarder for reversing the pathological structure of neuronal synapses.

Methods Seven weeks of standardized exercise at moderate intensity was carried out using an animal treadmill in the vehicle + Run and STZ + Run groups. Based on quantitative transcriptome and tandem mass tag (TMT) proteome sequencing, weighted gene co-expression analysis (WGCNA) and gene set enrichment analysis (GSEA) were used to investigate the activation of complement cascades to injury neuronal synaptic plasticity. Golgi staining, Western blotting, immunofluorescence staining, and electrophysiology were used to verify the reliability of sequencing data. The role of NDRG2 was assessed by overexpressing or inhibiting the NDRG2 gene *in vivo*. Moreover, we estimated the cognitive function in diabetic or normal patients using DSST scores.

Findings Exercise reversed the injury of neuronal synaptic plasticity and the downregulation of astrocytic NDRG2 in diabetic mice, which succeeded in attenuating DACD. The deficiency of NDRG2 aggravated the activation of complement C3 by accelerating the phosphorylation of NF-κB, ultimately leading to synaptic injury and cognitive dysfunction. Conversely, the overexpression of NDRG2 promoted astrocytic remodeling by inhibiting complement C3, thus attenuating synaptic injury and cognitive dysfunction. Meanwhile, C3aR blockade rescued dendritic spines loss and cognitive deficits in diabetic mice. Moreover, the average DSST score of diabetic patients was significantly lower than that of non-diabetic peers. Levels of complement C3 in human serum were elevated in diabetic patients compared to those in non-diabetic patients.

Interpretation Our findings illustrate the effectiveness and integrative mechanism of NDRG2-induced improvement of cognition from a multi-omics perspective. Additionally, they confirm that the expression of NDRG2 is closely related to cognitive function in diabetic mice and the activation of complement cascades accelerated impairment of neuronal synaptic plasticity. NDRG2 acts as a regulator of astrocytic-neuronal interaction via NF-κB/C3/C3aR signaling to restore synaptic function in diabetic mice.

Funding This study was supported by the National Natural Science Foundation of China (No. 81974540, 81801899, 81971290), the Key Research and Development Program of Shaanxi (Program No. 2022ZDLSF02-09) and Fundamental Research Funds for the Central Universities (Grant No. xzy022019020).

Abbreviations: AAV-Ctrl, rAAV-GfaABC1D-mCherry-WPRE-SV40-pA, AAV2/9; AAV-NDRG2, rAAV-GfaABC1D-NDRG2-2A-mCherry-WPRE-pA, AAV2/9; ACSF, Artificial cerebrospinal fluid; AD, Alzheimer's disease; AP, Anteroposteriorly; BDNF, Brain-derived neurotrophic factor; CNGBdb, China National GeneBank DataBase; DACD, Diabetes-associated cognitive dysfunction; DMEM, Dulbecco's modified Eagle's; DV, Dorsoventrally; GO, Gene Ontology; Gpld1, Glycosylphosphatidylinositol-specific phospholipase D1; GSEA, Gene set enrichment analysis; ME, Module eigengene; mEPSCs, Miniature excitatory postsynaptic currents; ML, Mediolaterally; MWM, Morris water maze; NDRG2, N-myc downstream regulatory gene 2; PCA, Principal component analysis; STZ, Streptozotocin; SYP, Synaptophysin; T1DM, Type 1 diabetes mellitus; TMT, Tandem mass tag; WB, Western blotting; WGCNA, Weighted gene co-expression analysis

*Corresponding author. Department of Anesthesiology & Center for Brain Science, The First Affiliated Hospital of Xi'an Jiaotong University, 277 Yanta West Road, Xi'an 710061, Shaanxi, China.
E-mail address: dr.wangqiang@xjtu.edu.cn (Q. Wang).
[e]Tao Jiang and Yansong Li share the first authorship.

Keywords: Diabetes; Cognitive dysfunction; NDRG2; Complement C3

Research in context

Evidence before this study

The incidence of diabetes-associated cognitive dysfunction (DACD) among diabetic individuals is currently 13.5%, which seriously impacts self-glycemic management and may lead to life-threatening complications, including hypoglycemia, hyperglycemic hyperosmotic coma, and ketoacidosis. Regular exercise promotes exercise-induced factors to stimulate the expression of brain-derived neurotrophic factor (BDNF), improve neuronal synaptic plasticity, and attenuate cognitive defects in patients with Alzheimer's disease (AD). Nonetheless, the regulatory role of exercise in astrocytic remodeling in cognitive dysfunction remains poorly understood.

NDRG2 is specifically expressed in astrocytes, and the abnormal expression of NDRG2 is closely related to the pathogenesis of many neurological diseases (e.g., glioma, stroke, AD, depression, and attention-deficit/hyperactivity disorder). However, whether the function of astrocytic NDRG2 is involved in the pathophysiology of DACD need to be further explored. Classical complement signaling is activated to regulate the proper synaptic formation, but control over this signaling is lost during aging and neurodegenerative diseases. Then, astrocytes acquire strong neurotoxicity and lose their function of promoting synaptic formation and pruning. Whether NDRG2 is involved in activating complement cascades and synaptic injury requires further exploration.

Added value of this study

This study examined the molecular pathway linking neuronal-astrocytic interaction to restore synaptic injury and cognitive dysfunction in diabetes. We found that the deficiency of NDRG2 aggravates the activation of complement C3 by accelerating the phosphorylation of NF-κB, ultimately reversing the protective effect of exercise on synaptic injury and cognitive dysfunction. Conversely, the overexpression of NDRG2 promotes astrocytic remodeling by inhibiting complement C3, alleviating synaptic injury and cognitive dysfunction. Meanwhile, C3aR blockade rescues dendritic spines loss and cognitive deficits in diabetic mice.

Implications of all the available evidence

We analyzed the integrative pathogenesis of DACD by conducting transcriptomic and TMT quantitative proteomic sequencing of hippocampal tissue from diabetic mice, which revealed that the activation of complement cascades accelerates the impairment of neuronal synaptic plasticity. Furthermore, we report that NDRG2 acts as a regulator of astrocytic-neuronal interaction via NF-κB/C3/C3aR signaling to restore synaptic function in diabetic mice.

Introduction

The worldwide prevalence of diabetes is predicted to exceed 640 million by 2040.[1,2] Furthermore, the incidence of diabetes-associated cognitive dysfunction (DACD) among diabetic individuals is currently 13.5%[3] and may is over 24.2% in those above 75 years old.[4] DACD is mainly characterized by diabetes-associated cognitive decrement, mild cognitive impairment, and dementia.[5] These symptoms seriously impact self-glycemic management and may lead to critical complications, including hypoglycemia, hyperglycemic hyperosmotic coma, and ketoacidosis. As the most serious stage of DACD, dementia is the second leading cause of death among individuals with diabetes.[6] Therefore, there is an immediate urgency to clarify the integrative pathophysiology of various metabolic disorders that result from diabetes.

Exercise is one of the five most impactful treatments for diabetes. It promotes building muscles, it strengthens immune function, and helps to improve sleep, mood, and memory. Studies have shown that regular exercise induces hepatogenic factors [glycosylphosphatidylinositol-specific phospholipase D1 (Gpld1)], metabolic factors (ketone body and lactate), and myogenic factors (Cathepsin-B and Irisin), stimulating the expression of brain-derived neurotrophic factor (BDNF), improving neuronal synaptic plasticity[7] and attenuating cognitive defects in elderly or those with Alzheimer's disease (AD).[8]

Astrocytes play a crucial role in promoting synaptic genesis or phagocytic pruning synapses,[9] uptaking or recycling neurotransmitters[10] and maintaining energy homeostasis.[11] Each astrocyte occupies a non-overlapping region, participates in neurovascular units,[12,13] and maintains neuronal support as an active component of tripartite synapses.[11] Nonetheless, the regulatory role of exercise on astrocytes in cognitive dysfunction is yet poorly understood.

As a member of the N-myc downstream regulatory gene (NDRG) family, NDRG2 is specifically expressed in astrocytes, regulating the clearance of glutamate[14] and participating in the integrity of the blood–brain barrier,[15] cell proliferation,[16] and differentiation.[17] The abnormal expression of NDRG2 is closely related to the

pathogenesis of many neurological diseases (e.g., glioma,[18] stroke,[19,20] Alzheimer's disease,[21] depression,[22] and attention-deficit/hyperactivity disorder[14]). In addition, NDRG2 deficiency results in the accumulation of interstitial glutamate and increased neuroexcitatory transmission, which contributes to abnormal behaviors and impaired memory.[14] Loss of NDRG2 worsened cognitive dysfunction in AD mice by reducing the levels of proteasome subunit PSMB6, an essential enzyme for the degradation of Aβ and tau.[21] However, whether the function of astrocytic NDRG2 is involved in the pathophysiology of DACD remains unclear.

Astrocytes secrete positive or negative glial factors to promote synaptogenesis[23,24] or phagocytosis and pruning of synapses,[25] which are processes essential for neural homeostasis related to cognition and memory.[26,27] Classical complement signaling is activated to regulate the synaptic formation; yet, the control over this signaling is lost during aging and neurodegenerative diseases.[9,28,29] The activation of microglia initiates this signaling, secreting C1q, Il-1α, and TNF-α, which induce the formation of the C1 complex (C1q, C1r, and C1s) and cleave C4 and C2 to form C4b2b (a C3 invertase). Then, complement C3 is upregulated and cleaved into C3a and C3b.[30,31] Finally, C3a binds with C3aR to promote microglial activation and neuronal synaptic pruning.[32] In cases of neurodegenerative diseases, astrocytes acquire strong neurotoxicity[9,33] and lose their function of promoting synaptic formation and pruning.[28,29] In this study, we aim to explore the protective effect of exercise on DACD and identify NDRG2 as a potential guarder for reversing the pathological structure of neuronal synapses by inhibiting p-NF-κB and C3.

Methods

Study design

According to established protocols,[34] seven weeks of standardized exercise at moderate intensity was carried out using an animal treadmill (ZH-PT, Anhui, China) in the vehicle + Run and STZ + Run groups. The exercise was performed for 30 min over five consecutive days every week. The speed parameters included a velocity of 5–8 m/min and acceleration of 4 m/s^2. Vehicle and STZ groups not subjected to exercise training were free to access water and food. According to the randomization principle, we used a random number table for designing the experiment.

Animals

C57BL/6 mice, 8–10-week-old, weighing 21–22 g, were obtained from the Experimental Animal Center of Xi'an Jiaotong University and maintained under specific pathogen-free conditions environment with a temperature of 22 ± 1 °C, relative humidity of 50 ± 1%, and a light/dark cycle of 12/12 h and had free access to water and food. Type 1 diabetes mellitus (T1DM) was induced by administrating streptozotocin (STZ) (Sigma–Aldrich, USA). First, STZ was dissolved in sterile, freshly prepared 0.1 M citric acid buffer (pH = 4.5). For five consecutive days, the diabetic mice were intraperitoneally injected with 50 mg/kg STZ, while the vehicle mice were intraperitoneally injected with 0.1 M citric acid buffer. After two weeks, random blood glucose was measured in the tail vein using a Roche glycemic meter. Mice with random blood glucose value >16 mmol/L were considered diabetic. The sacrifice time point of vehicle, STZ, vehicle + Run and STZ + Run groups was the same even at 23 weeks.

C3aR antagonist was purchased from Calbiochem (catalog No. SB290157). The 16-week-old vehicle and STZ mice were intraperitoneally (i.p.) injected with PBS or C3aRA (1 mg/kg) three times per week for three weeks. According to previous studies, mice were used for behavioral experiments at 20–23 weeks; at that time, they displayed symptoms of diabetes-associated cognitive dysfunction.

Generation of acNDRG2 KO and NDRG2 overexpression

Ndrg2$^{fl/fl}$ mice were purchased from Cyagen Biosciences, China. We performed stereotactic injection of rAAV-GFAP-CRE-WPRE-hGH into the hippocampal CA1 area of Ndrg2$^{fl/fl}$ mice, in which NDRG2 was conditionally deleted as an acNDRG2 KO, and stereotactic injection of rAAV-GFAP-EGFP-WPRE-hGH (AAV-GFP) in control group mice.[35] To overexpress NDRG2, we injected rAAV-GfaABC1D-NDRG2-2A-mCherry-WPRE-pA, AAV2/9 (AAV-NDRG2) into the hippocampal CA1 area of both vehicle and STZ mice, forming a vehicle + AAV-NDRG2 and STZ + AAV-NDRG2 groups. As a control, we injected rAAV-GfaABC1D-mCherry-WPRE-SV40-pA, AAV2/9 (AAV-Ctrl) into the CA1 area of vehicle and STZ mice, forming a vehicle + AAV-Ctrl and STZ + AAV-Ctrl mice.

The viruses, rAAV-GfaABC1D-NDRG2-2A-mCherry-WPRE-pA, AAV2/9; rAAV-GfaABC1D-mCherry-WPRE-SV40-pA, AAV2/9; rAAV-GFAP-CRE-WPRE-hGH and rAAV-GFAP-EGFP-WPRE-hGH were constructed and purchased from BrainVTA (Wuhan) Co., Ltd, China. Stereotactic virus injection was performed according to the following steps: mice were anesthetized with isoflurane and their heads were fixed in a stereotactic apparatus (RWD, Shenzhen, China). An appropriate amount of erythromycin eye ointment was then applied to the eyes to prevent conjunctival infection. A small craniotomy was performed, exposing the Bregma point of the skull. Mice were bilaterally microinjected in the following sites: anteroposteriorly (AP) −1.5 mm from the Bregma point, mediolaterally (ML) ±1 mm, and dorsoventrally (DV) −1.55 mm to cover the dorsal CA1. Microinjections were carried out using a 5 μl syringe and a 33-gauge metal needle (65460-02, Hamilton, USA). According to the instruction, the viral titer was

≥2.00E + 12 vg/mL. The flow rate (24 nL/min) was controlled by an injection pump for 10 min to inject 240 nL. Then, we stopped the needle, waited an additional 10 min to allow the viral vector to diffuse away from the needle track, and slowly withdrew the needle over another 5 min. After suturing the incision, mice recovered on an electric blanket for postoperative care.

Transcriptomic sequencing and WGCNA analysis

Total RNA was extracted from the hippocampi of vehicle, STZ, and Run + STZ mice using a TRIzol reagent kit. RNA quality was verified by the Nano Drop ND-1000, and RNA was reverse-transcribed to cDNA using Super Script™ II Reverse Transcriptase reagent (1896649, Invitrogen). Then cDNA was then used to synthesize U-labeled second-stranded DNAs. Ultimately, 2 × 150 bp paired-end sequencing (PE150) was performed on the Illumina Novasequencing™ 6000 (LC-Bio Technology Co., Hangzhou, China).

The mRNA transcripts were processed using String Tie and ballgown (http://www.bioconductor.org/packages/release/bioc/html/ballgown.html) to arrive at 55,450 total genes. Weighted gene co-expression network analysis (WGCNA) of transcriptomic data was used to construct a hierarchical cluster tree, in which differently colored branches represent the 18 gene modules.[36] To satisfy the correlation of genes that conformed to scale-free topological distribution, the soft threshold β adopted a scale-free topological fitting index >0.8 or the minimum β value when reaching the plateau stage. The minimum number of genes and merged cut height was set to 30 and 0.4, respectively. The principal component 1 (PC1) of each module in principal component analysis (PCA) represents module eigengene (ME), which reflects the characteristics of overall gene expression in this module. The correlation network was obtained by calculating the ME correlation-ship among different modules.

TMT proteomic sequencing and GSEA analysis

TMT proteomic sequencing was performed according to the previous protocols.[37] The hippocampi of vehicle, STZ, and Run + STZ mice were lysed and homogenized by SDT buffer and auto homogenizer using a velocity of 6.0 M/S three times for 30 s each.[38] After being boiled for 15 min, the samples were centrifuged at 14000 g for 15 min. The filtrate was obtained from 0.22 μm filters and quantified using a BCA Kit (23225, Thermo Fisher). The 20 μg proteins were then separated by SDS-PAGE gel for quality measurement, and 200 μg proteins were digested according to the instructions of Filter-Aided Sample Preparation (FASP digestion).[37] Then, 100 μg of peptides from each sample were labeled using TMT reagent and then fractionated by the Agilent 1260 Infinity II HPLC.

We selected the Uniprot_MusMusculus_17027_20200226 database for qualitative analysis and acquired 295,274 total spectra with 114,660 peptide spectra matches after screening out 53,640 unique peptides and 6557 proteins. The traditional KEGG or GO analysis relied on defined difference thresholds: fold change >1.2 or <0.83 and p-value <0.05. However, Gene Set Enrichment Analysis (GSEA) integrated most gene expression characteristics in the predefined gene set,[39] which could detect a large number of functional genes with no statistically significant differences. According to the expression ratio, ALL genes followed the distribution of predefined gene set S and were randomly distributed or concentrated at the top or bottom of the list. Herein, the GSEA of transcriptomic and proteomic data was carried out in the Lian-Chuan Bio-Cloud Platform. The predefined gene set was C2.Cp.KEGG.v7.1.

Data availability

Transcriptomic and proteomic sequencing data that support our study findings are original and stored in CNSA (https://db.cngb.org/cnsa/) of CNGBdb (China National GeneBank DataBase) with accession number CNP0002799.

Golgi staining

After various experimental treatments, mouse brains were collected. The hippocampus was cut into 2–3 mm blocks and immersed in Golgi solution for 48 h—Golgi solution was changed once every three days for a total of 14 days. Then, samples were dehydrated in 15% sucrose solution for one day and 30% sucrose solution for 2 day at 4 °C in dark. After treatment with concentrated ammonia water and fixing solution, samples were further dehydrated for two to three days, then frozen and sliced into 100 μm sections which were sealed with glycerin gelatin. Images were captured as soon as possible using a super-resolution confocal microscope (Leica TCS SP8 STED 3X). Sholl analysis was used to examine the total dendritic length and neuronal complexity, while Imaris analysis was applied to reconstruct the 3D structure of dendritic spines by automatic classification.

Electrophysiology

Analysis of miniature excitatory postsynaptic currents (mEPSCs) was performed to observe neuronal synaptic transmission.[40] After being anesthetized by isoflurane, mice were subjected to perfusion with an oxygenated (95% O_2/5% CO_2) cutting solution consisting of the following reagents: 2.5 mM KCl, 120 mM choline chloride, 7 mM $MgCl_2$, 1.25 mM NaH_2PO_4, 0.5 mM $CaCl_2$, 5 mM sodium ascorbate, 26 mM $NaHCO_3$, 3 mM sodium pyruvate, and 25 mM glucose. Then, brains were prepared into 300 μm hippocampal slices using a VT1200S Vibratome (Leica Microsystems). Slices were transferred into the cutting solution at 34 °C for 15 min and transferred into the incubator with artificial cerebrospinal fluid (ACSF), containing 2.5 mM KCl,

124 mM NaCl, 2 mM $MgSO_4$, 1.25 mM NaH_2PO_4, 2.5 mM $CaCl_2$, 10 mM glucose, and 26 mM $NaHCO_3$. Slices were then incubated at 25 ± 1 °C for at least 1 h. Whole-cell patch-clamp recordings of CA1 pyramidal neurons were conducted at –70 mV in the presence of 100 μM picrotoxin and 1 μM TTX for mEPSC recording. The pipette solution contained the following reagents: 5 mM KCl, 125 mM K-gluconate, 10 mM HEPES, 1 mM $MgCl_2$, 0.2 mM EGTA, 4 mM Mg-ATP, 0.3 mM Na-GTP, and 10 mM phosphocreatine (pH 7.35, 290 mOsm). Signals were acquired using a MultiClamp 700B amplifier and 1550A digitizer (Molecular Devices). To obtain a high signal-to-noise ratio and accurately determine the mEPSC amplitude, only event >10 pA was accepted for analysis. Data were collected with pClamp 10.0 software (Molecular Devices).

Y-maze

Y-maze (30 cm × 6 cm × 15 cm) testing was used to evaluate spatial working memory.[41] The maze consisted of an isolated triangular central area and three identical arms at an angle of 120. The mice were allowed to explore the Y-maze for 8 min freely. If they could accurately remember the directions they came from, the correct alternation order was ABC or another sequence of three non-repeated arms. If they could not remember these directions, the alternation order would include at least two repeated arms (i.e., ABB, ABA, ACA, or ACC). Therefore, spontaneous alternation (%) was calculated using the following equation: spontaneous alternation (%) = correct alternation/(total arm entries–2) × 100. Meanwhile, the total arm entries and total distance parameters reflected autonomous movement ability. To ensure consistent and reliable experimental data, the surrounding environment was kept quiet, and the experiment was performed during the same period each day.

Morris water maze (MWM)

The Morris water maze consisted of a thermostatic swimming pool at a temperature of 20–25 °C. Four shapes (circle, square, diamond, and triangle) were pasted on the four sides of the maze. A hidden platform was located 0.5 cm lower than the water's surface in the fourth quadrant. During the five training days, mice were gently placed into the water from the four marked directions. Escape latency to the hidden platform and swimming velocity were recorded using a WMT-100 Morris system. On the last day, the hidden platform was removed. The number of platform crossovers and target quadrant retention time (%) were observed to evaluate spatial learning memory.[42]

Western blotting

Hippocampal samples were harvested and weighed (0.015–0.02 g), then homogenized in 150–200 μl of fresh, ice-cold RIPA lysis buffer (Beyotime, Nantong, China) containing protease inhibitor and phosphatase inhibitor. The samples were stirred by an electric grinder for 3 s × 4 times on the ice, crushed with an ultrasonic cell crusher for 4 s × 4 times, and centrifuged at 12000 rcf for 10 min. The supernatant was taken for protein quantification and diluted to a protein concentration of 3 μg/μl. Samples were then incubated with the following primary antibodies: anti-C3 rabbit monoclonal antibody (ab200999, Abcam, UK), anti-PSD95 mouse monoclonal antibody (ab13552, Abcam, UK), anti-SYP rabbit monoclonal antibody (ab32127, Abcam, UK), anti-NDRG2 rabbit monoclonal antibody (5667-WB, CST, USA), anti-NF-κB rabbit monoclonal antibody (ab32536, Abcam, UK), anti-p-NF-κB rabbit monoclonal antibody (3033T, CST, US), and anti-β-tubulin mouse monoclonal antibody (66240-1-lg, Proteintech, China) at 4 °C overnight.

Cell culture

C57BL/6J mice pups at 2–3 days were prepared to culture primary astrocytes, and fetal mice at 14–16 days were prepared to culture primary neurons. After anesthesia, the brain tissues were stripped out in Dulbecco's modified Eagle's (DMEM). Under the microscope, brain meninges were removed by a precision instrument, and the hippocampus was minced by ophthalmic scissors. Then, 0.25% trypsin 2–3 mL was added to digest tissues for 10 min, and the cell suspension was filtered with 75 μm nylon mesh. The cells were counted and seeded into poly-Dlysine-coated culture flasks in a humidified atmosphere containing 5% CO_2/95% air at 37 °C. After 7–9 days, the astrocytes were purified (190–200 rpm/min, 18 h–20 h, 37 °C constant temperature shaking table) and inoculated for experimental treatment: normal glucose NG5.5 mmol/L (serum-free DMEM containing 5.5 mmol/L D-glucose, 10% fetal bovine serum (Gibco, USA), 50 U/mL penicillin and 50 mg/mL streptomycin); high glucose HG55 mmol/L (serum-free DMEM containing 55 mmol/L D-glucose, 10% fetal bovine serum (Gibco, USA), 50 U/mL penicillin and 50 mg/mL streptomycin). We applied LV-NDRG2 to overexpress NDRG2 in primary astrocyte and LV-GFP as a control. We used LV-shRNA-NDRG2 to downregulate NDRG2 in primary astrocyte and LV-scramble as a control. LV-NDRG2, LV-GFP, LV-shRNA-NDRG2 and LV-scramble were constructed and purchased from Hanbio Biotechnology Co. Ltd. (Shanghai, China). The treatment of the BAY11–7082 (BAY, 5 μM, MCE, Monmouth Junction, NJ, USA) was used to inhibit the activation of NF-κB.

Immunofluorescence staining and ELISA

After being gradient dehydrated by 20% and 30% glucose, brains were embedded with OCT glue and frozen in a cryostat (Cryostar NX50™, Thermo Scientific) for over 1 h. The frozen brain was prepared into 16 μm thick sections, then incubated with goat serum containing 0.2% Trion-100 at 37 °C for 30 min. NDRG2 labeling was performed by incubating with primary anti-NDRG2

rabbit monoclonal antibody (ab174850-IF, Abcam, UK), anti-GFAP chicken polyclonal antibody (GTX85454, Gene Tex, USA), and anti-NeuN mouse monoclonal antibody (MAB377, Merck Millipore, USA) overnight at 4 °C. The sections were then washed with PBS (phosphate-buffered saline) for 7 min × 3 times. The next day, sections were incubated for 2 h with fluorescent secondary antibodies Alexa Fluor®488 (139424, Jackson Immuno, USA), Alexa Fluor® 594 (ab150064, Abcam, UK), and Alexa Fluor® 647 (ab150115, Abcam, UK). DAPI was added during the final 5 min of incubation. The sections were stored at 4 °C until observed, and images were captured as soon as possible using a confocal fluorescence microscope (BX51, Olympus, Tokyo, Japan) or super-resolution confocal microscope (Leica TCS SP8 STED 3X). Insulin concentration was detected according to the instructions of a Mouse INS (Insulin) ELISA Kit (E-EL-M1382c) purchased from Elabscience, Wuhan, China.

Ethics approval

All animal studies (including the mice euthanasia procedure) were done in compliance with the regulations from the Ethics Committee of animal research of Xi'an Jiaotong University (protocol No. 2019-060) and conducted according to the ARRIVE, AAALAC and IACUC guidelines. We used minimized animals to satisfy statistical requirements. According to advanced experimental results, we calculated the standard deviation and sample mean to estimate the required sample size. The sample size of MWM tests in vehicle and STZ groups was calculated as follow. According to our advanced experimental results of platform crossover, the standard deviation = 1.563 and mean difference = 2.478. $\alpha = 0.05$, two-sided, $Z\alpha = Z_{0.05} = 1.96$, test efficacy β is unilateral, $\beta = 0.9$, $Z_\beta = 1.28$. Based on these values, a sample size of 8.3528 per group provided 90% power with a type I error α of 0.05. Considering the 20% loss rate, we included 10 mice in vehicle group and 9 mice in STZ group. Simultaneously, the literature showed that the sample size of behavioral tests was mostly 5–10 mice/group, Western blotting (WB) consisted of 6 mice/group, immunofluorescence staining was 3 mice/group, and transcriptome and proteome data were based on 3–5 mice/group.[9,43,44] We also referred to these studies for calculation to minimize the required sample size. The clinical protocol was approved by the Ethics Committee of the First Affiliated Hospital of Xi'an Jiaotong University (ID: ChiCTR1900021720). All subjects obtained the informed consent of their participation in this study.

Subjects and clinical assessments

To analyze the possible risk factors of diabetes-associated cognitive dysfunction in humans, we recruited 40 subjects consisting of 27 diabetic individuals (17 male and 10 female, mean age 68.963 years) and 13 non-diabetic individuals (10 male and 3 female, mean age 66.6923 years). The inclusion criterion were those >60-year-olds who either met the American Diabetes Association criteria for diagnosis of diabetes or did not (healthy controls) from the First Affiliated Hospital of Xi'an Jiaotong University. The exclusion criteria removed patients affected by infection or inflammation or had other clinically diagnosed mental disorders. We assessed cognitive function using DSST scores and collected serum and metabolic indicators for correlation analysis. We used https://clincalc.com/stats/samplesize.aspx software to calculate the sample size. According to our advanced experiment of DSST scores, we calculated standard deviation $\boldsymbol{\sigma} = 8.31$ and mean difference between two groups $\boldsymbol{\delta} = 11$. The calculation formula for human sample size between two groups was: $n = \frac{(Z_\alpha + Z_\beta)^2 * 2\sigma^2}{\delta^2}$ $\alpha = 0.05$, two-sided, $Z\alpha = Z_{0.05} = 1.96$, test efficacy β is unilateral, $\beta = 0.9$, $Z_\beta = 1.28$. Based on these values, a sample size of 11.98 per group provided 90% power with a type I error α of 0.05. In order to minimize sampling error and make the sample representative, we randomly included 13 patients in the normal group and 27 patients in the diabetic group. The Human C3 (Complement Component 3) ELISA Kit (E-EL-H6054) and Human INS (Insulin) ELISA Kit (E-EL-H2665c) were purchased from Elabscience, Wuhan, China. Measurements of C3 and insulin were performed according to the manufacturer's instructions.

Statistical analysis

GraphPad Prism Version 7.0 software was used for statistical analysis. All values were expressed as mean ± SEM unless otherwise stated and were performed the Normality test. The normality test was carried out by Shapiro–Wilk normality test to check whether the variables in this study were consistent with normal distribution. Comparisons between two groups were analyzed using a two-tailed Student's t-test. Two-way ANOVA with Tukey's multiple comparisons tests analyzed the escape latency in the MWM test and the body weight fluctuation. One-way ANOVA with Tukey's multiple comparisons tests analyzed other values among four groups. PCA analysis is based on the correlation between variables to decompose, merge, and reduce dimensions. In this study, PCA analysis was carried out based on all gene expression values in the module, and the PC1 value was the weighted value of all gene expression levels. The PC1 value can accurately characterize the overall expression characteristics of module genes, termed module eigengene (ME). Correlation analysis was carried out using ME to obtain a correlation network of different modules. We applied univariable logistic regression to assess the associations between risk factors and DSST scores. We also conducted multivariate logistic regression analysis in the SPSS (Tables 2–5). $^{*}p < 0.05$, $^{**}p < 0.01$, $^{***}p < 0.001$, $^{****}p < 0.0001$, $^{\#}p < 0.05$, and $^{\#\#}p < 0.01$ were considered statistically significant.

Role of the funders

This study was supported by the National Natural Science Foundation of China (No. 81974540, 81801899, 81971290), the Key Research & Development Program of Shaanxi (Program No. 2022ZDLSF02-09) and Fundamental Research Funds for the Central Universities (Grant No. xzy022019020). These funders were not involved in any aspects regarding conduction, analysis, interpretation, or publication of the study.

Results

Exercise attenuates cognitive dysfunction and enhances the expression of neuronal synaptic plasticity genes in diabetic mice

Since high-intensity exercise may lead to acute diabetic complications such as ketoacidosis, we carried out seven weeks of standardized exercise at moderate intensity and observed learning memory defects in diabetic mice (Fig. 1a). Random blood glucose level, HOMA-IR value, and food & water intake were higher in diabetic mice compared to non-diabetic mice. Body weight was lower in the diabetic group compared to the non-diabetic group at baseline, but these observations were reversed by exercise (Fig. S1a–f). In the open field test, the entries, distance, and time in the center zone showed no significant differences between STZ and vehicle groups (Fig. S1g–k), while the entries and distance in the center zone were increased after exercise in v + Run mice compared with the vehicle group (Fig. S1h and i), indicating that exercise promotes the exploration behavior.

Furthermore, we performed Y-maze and Morris water maze (MWM) behavioral tests to observe learning memory defects in diabetic mice. The alternation triplet (%) was decreased in diabetic mice, whereas exercise improved the alternation triplet (%) in STZ + Run mice at Y-maze (Fig. 1b). Meanwhile, there were no remarkable differences in total arm entries or total distance among each group (Fig. 1c and Fig. S1l). In the MWM test, escape latency was delayed in diabetic mice, while platform crossover and target quadrant retention time (%) were decreased in the STZ group. These deficiencies were rescued by exercise in the STZ + Run group (Fig. 1d–g). In addition, there were no significant differences in swimming velocity among groups (Fig. S1m). Together, these results indicate that exercise alleviates abnormal metabolic signs and improves hippocampal-dependent learning memory in diabetic mice.

Next, we analyzed the hippocampal tissue from the vehicle, STZ, and STZ + Run groups for quantitative transcriptomic sequencing. A total of 2664 differentially expressed genes were identified by filtering with fold change >2 or <0.5 and p-value <0.05 in DESeq2 analysis (http://www.bioconductor.org/packages/release/bioc/html/DESeq2.html). Principal component analysis (PCA) of the 15 samples indicated that the distributions of samples among the three groups was discrete and different from each other, whereas the distribution of samples within each group was aggregative and consistent (Fig. 1i). This result confirmed the good consistency of the samples within the group. Next, we performed a weighted gene co-expression network analysis (WGCNA) of the 55,450 total genes from the 15 independent samples. A soft threshold of 0.8 and merged cut height of 0.4 were used to ensure that the gene correlation network satisfied the scale-free-topological distribution. Consequently, we obtained a cluster dendrogram with 18 modules from WGCNA (Fig. 1h). Then, a hierarchical cluster tree was constructed, wherein differently colored branches represent the 18 gene modules.

PCA analysis of the 18 modules confirmed that the distribution of the modules was dispersed, representing different groups of genes based on the biological function (Fig. 1j). Principal component 1 (PC1) value reflected weighted gene expression patterns in each module, termed the module eigengene value. The correlation network was obtained by calculating module eigengene correlation-ship among different modules (Fig. 1k). Next, we demonstrated the biological functions of 18 modules by Gene Ontology (GO) enrichment analysis of each module. The cellular nature of each module was clarified by checking whether it consisted of specific cell-type biomarkers, and hub genes were identified according to the weighted value of each gene. The module eigengene for module 1 was clearly decreased in diabetic mice, and it was moderately improved after exercise (Fig. 1l). In addition, enrichment of neuronal synaptic plasticity genes—*Syt 1, Manf, Syp, and Bdnf*—was observed in module 1 (Fig. 1m). These results demonstrated that exercise may reverse the declined expression of neuronal synaptic plasticity genes in diabetic mice.

Exercise restores the impairment of neuronal synaptic plasticity in the diabetic hippocampus

To validate the neuronal morphology of diabetic mice, we evaluated neuronal complexity and classified the 3D structure of dendritic spines. The total dendritic length and neuronal complexity were lower in diabetic compared to those in non-diabetic mice but were preserved after exercise in STZ + Run mice (Fig. 2a–c and Fig. S1p). The reconstruction of dendritic spines demonstrated that total spine density was obviously reduced in diabetic mice, especially in stubby and mushroom spines. On the other hand, exercise (STZ + Run group) increased the total spine density of stubby and mushroom spines (Fig. 2d–g).

Meanwhile, we also examined whether diabetes impacted the expression of synaptic proteins. The expression levels of excitatory postsynaptic density marker PSD-95 and presynaptic density marker synaptophysin (SYP) were decreased in diabetic compared to those in non-diabetic mice, and this deficit was rescued by exercise in STZ + Run mice (Fig. 2h and i). Consistent with the

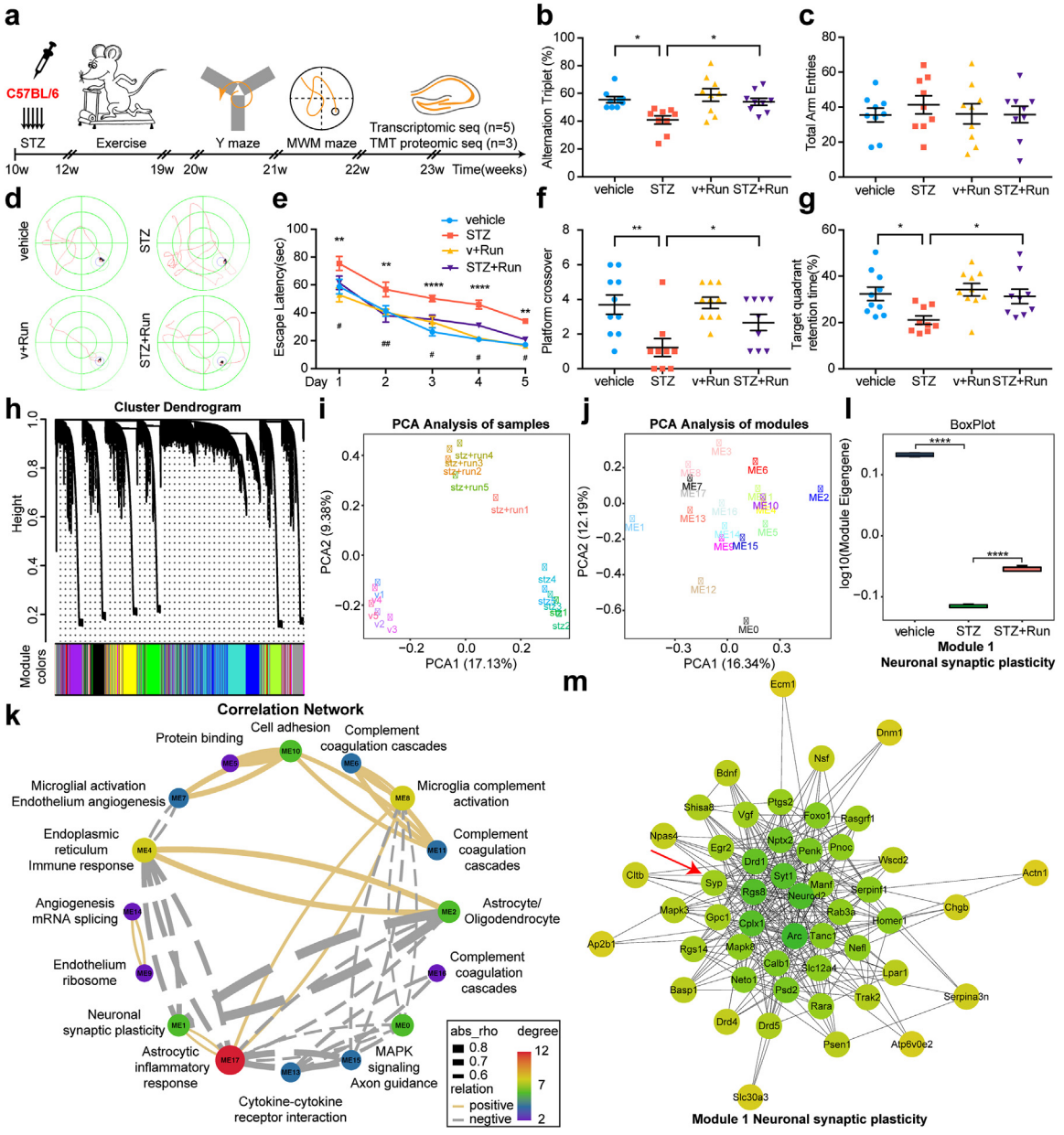

Fig. 1: **Transcriptomic analysis revealed the protective effect of exercise and the integrative pathogenesis of DACD. (a)** Schematic that represents the chronological order of STZ injection, exercise, cognitive testing, and omics analysis. **(b)** The alternation triplet (%) of Y-maze was decreased in STZ group compared with vehicle mice (*p = 0.0145 between vehicle and STZ), which was reversed by exercise (n = 9/group) (*p = 0.0339 between STZ and STZ + Run). **(c)** Y-maze total arm entries (n = 9/group). **(d)** Representative traces of diabetic or non-diabetic mice after exercise in MWM test. **(e)** Escape latency of the MWM test was delayed in STZ mice compared with vehicle (**p = 0.004 **(day 1)**, **p = 0.0077 **(day 2)**, ****p < 0.0001 **(day 3)**, ****p < 0.0001 **(day 4)**, **p = 0.0028 **(day 5)** between vehicle and STZ), which was rescued after exercise (n = 10 vehicle and v + Run, n = 9 STZ and STZ + Run) ($^{\#}p$ = 0.0282 **(day 1)**, $^{\#\#}p$ = 0.001 **(day 2)**, $^{\#}p$ = 0.0154 **(day 3)**, $^{\#}p$ = 0.0151 **(day 4)**, $^{\#}p$ = 0.0391 **(day 5)** between STZ and STZ + Run). **(f–g)** The platform crossover (**f**) and target quadrant retention time (%) (**g**) during the probe trial of the MWM test were decreased in STZ mice compared with the vehicle group (**p = 0.0016 (**f**), *p = 0.0158 (**g**) between vehicle and STZ), which were upregulated after exercise (n = 10 vehicle and v + Run, n = 9 STZ and STZ + Run) (*p = 0.0444 (**f**), *p = 0.0359 (**g**) between STZ and STZ + Run). **(h)** Cluster dendrogram of WGCNA in transcriptome showing the 18 modules, distinguished by different colors (n = 5/group). **(i)** PCA analysis of transcriptomic samples. **(j)** Multidimensional distribution of 18 modules by PCA analysis. **(k)** Correlation network demonstrating the major cell types and Gene Ontology enrichments for each module and the relationships from a multidimensional perspective. Yellow represents a positive correlation, and grey represents a negative correlation. **(l)** The module eigengene of module 1 was downregulated at diabetic mice (****p < 0.0001 between vehicle and STZ), which was reversed by exercise (n = 5/group) (****p < 0.0001

alteration of neuronal morphology and dendritic spine density, the frequency of mEPSCs were abnormally elevated in diabetic compared to non-diabetic mice, which was obviously attenuated by exercise (Fig. 2j–l). However, there was no difference in the amplitude of mEPSCs among the groups (Fig. 2m and n). These findings illustrate that exercise ameliorates several impairments in synaptic plasticity and cognition in diabetic mice.

Exercise reverses the diabetes-induced decline of NDRG2 in astrocytes

The transcriptomic WGCNA revealed that astrocytic and oligodendrocytic genes—*Lcn2*, *Ndrg2*, and *Mobp*—were enriched in module 2 (Fig. 3a). We also identified a highly negative correlation between module 1 and module 2, indicating that astrocytic and oligodendrocytic genes might play a negative role in the neuronal synaptic plasticity of diabetic mice (Fig. 1k and Fig. S2a).

Although omics provided details for an integrated mechanism from a macro perspective, it was also critical to verify the reliability of our results at a micro level. Accordingly, we sought to assess the expression of NDRG2 in the hippocampus by performing confocal microscopy. We observed that NDRG2 mainly colocalized with astrocytic maker GFAP but not with neuronal marker NeuN. Furthermore, the confocal results showed that the intensities of NDRG2 in STZ groups were weaker than that of the vehicle group, which were fully rescued after exercise (Fig. 3b and c). In addition, we also found that the NDRG2 protein level was decreased in the STZ group compared to vehicle mice, and exercise led to a significant increase in the expression of NDRG2 in the STZ group by Western blotting (Fig. 3d and e). Together, these results indicate that astrocytic NDRG2 may act as an exercise-activated guarder for diabetes-associated cognitive dysfunction.

NDRG2 deficiency aggravates dendritic spine loss and cognitive dysfunction in diabetic mice

To acquire astrocyte-specific conditional NDRG2 knockout mice (acNDRG2 KO), $Ndrg2^{fl/fl}$ mice were obtained in which NDRG2 was conditionally deleted in a Cre-mediated pattern in astrocytes. We injected rAAV-GFAP-CRE-WPRE-hGH into the hippocampi of $Ndrg2^{fl/fl}$ mice and also injected rAAV-GFAP-EGFP-WPRE-hGH (AAV-GFP) into another group to serve as a control (Fig. 4a). We validated acNDRG2 KO by immunostaining, with the results showing an absence of NDRG2 in the astrocytes (Fig. 4b). Then, Western blotting was performed to clarify the effectiveness of NDRG2 deficiency (Fig. 6g–i). Although no significant differences in the escape latency were observed among each group (Fig. 4c), the platform crossover and target quadrant retention time (%) were decreased in the STZ + Run + acNDRG2 KO group (Fig. 4d and e). Similar to the results of MWM, STZ + Run + acNDRG2 KO may only affect long-term spatial learning memory. Herein, we did not observe the difference between STZ + Run + Control/acNDRG2 KO groups in short-term working memory in the Y maze test (Fig. S1q). The results of the classification of dendritic spines showed that STZ + Run + acNDRG2 KO mice experienced an accelerated reduction of stubby, mushroom, and long thin spine density, as well as total spine density, compared to STZ + Run + control mice (Fig. 4f–k). Above all, NDRG2 deficiency was found to block the protective effect of exercise on dendritic spines and cognitive function in diabetic mice.

Overexpression of NDRG2 alleviates synaptic injury and cognitive dysfunction in diabetic mice

We attempted to overexpress NDRG2, show the accuracy of stereoscopic injection, and clarify the effectiveness of rAAV-GfaABC1D-NDRG2-2A-mCherry-WPRE-pA, AAV2/9 (AAV-NDRG2). After the AAV-NDRG2 was injected into the hippocampus of the STZ group, the expression of NDRG2 increased (Fig. 5a and b), which was further confirmed by Western blotting (Fig. 6l). Working and spatial memory were then assessed using Y-maze and MWM testing. Although there were no significant differences in Y-maze total arm entries and total distance among the four groups, the alternation triplet (%) was decreased in the STZ + AAV-Ctrl group compared to the vehicle + AAV-Ctrl group, and was increased with overexpression of NDRG2 in the STZ + AAV-NDRG2 group (Fig. 5c–e). In the MWM tests performed at three to five days, escape latency was delayed in the STZ + AAV-Ctrl group compared to the vehicle + AAV-Ctrl group, whereas NDRG2 overexpression clearly shortened escape latency in the STZ + AAV-NDRG2 group (Fig. 5f and g). There were no significant differences in swimming velocity between the groups (Fig. 5h). Platform crossover and target quadrant retention time (%) were decreased in the STZ + AAV-Ctrl group compared to the vehicle + AAV-Ctrl group, and this deficit was rescued in the STZ + AAV-NDRG2 group (Fig. 5i and j). These results indicate that NDRG2 overexpression improves hippocampal-dependent memory in diabetic mice.

Moreover, the expression levels of PSD95 and SYP were decreased in the STZ + AAV-Ctrl group compared to those in the vehicle + AAV-Ctrl group, while these

between STZ and STZ + Run). **(m)** Module 1 enriched neuronal synaptic plasticity genes: Syt 1, Manf, Syp, and Bdnf. Values are presented as mean ± SEM. One-way ANOVA with Tukey's multiple comparisons test was performed in **b, f, g, l**. Two-way ANOVA with Tukey's multiple comparisons test was performed in **e**.

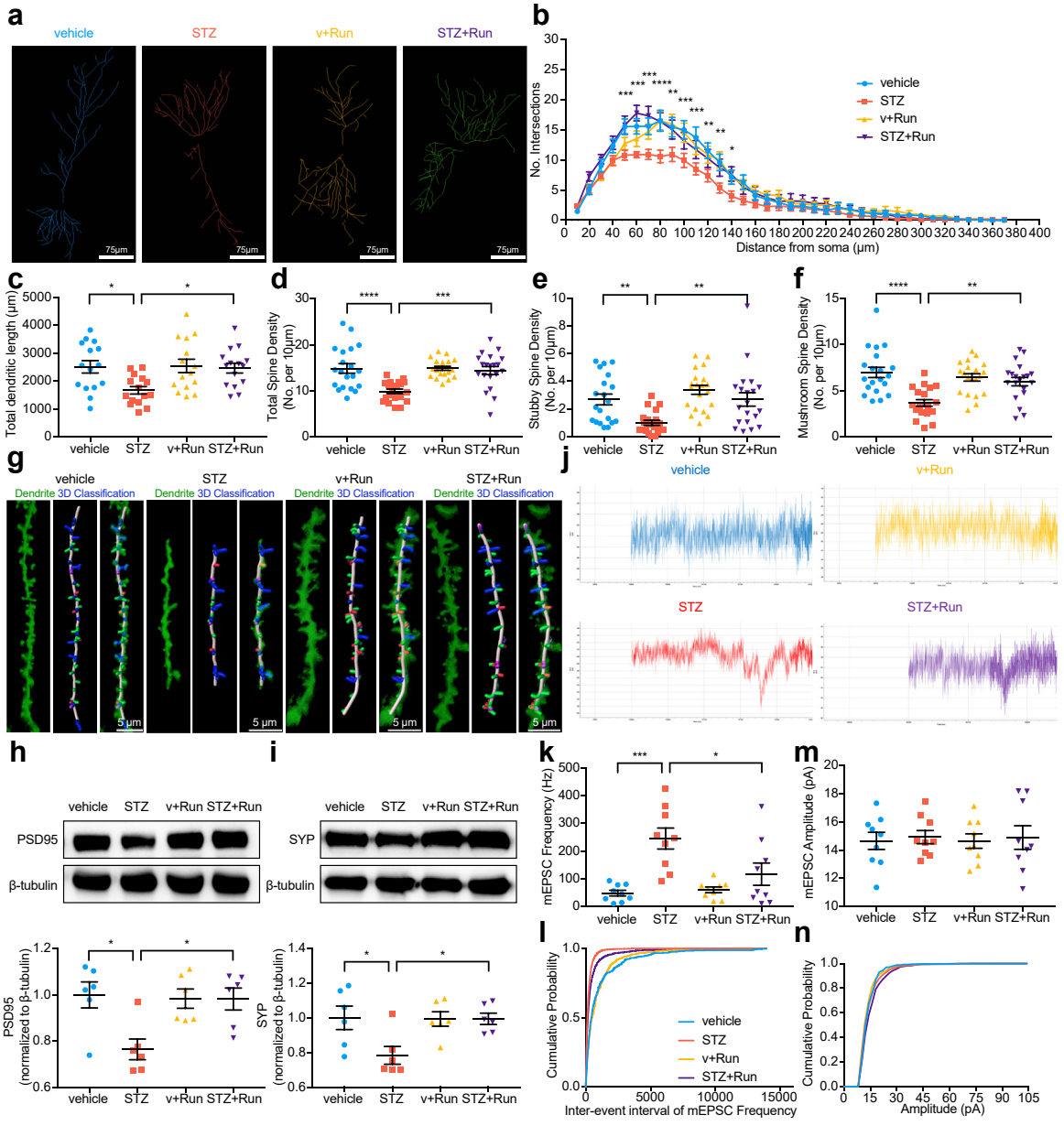

Fig. 2: **Exercise promotes neuronal morphology and function in diabetic mice. (a)** Representative images of neuronal dendritic morphology. Scale bar, 75 μm. **(b–c)** Quantification of dendritic complexity **(b)** and total dendritic length **(c)** by Sholl analysis exhibited a decline in the STZ group compared with vehicle mice (*p = 0.0192 between vehicle and STZ), which was increased after exercise (n = 15/group) (*p = 0.0297 between STZ and STZ + Run). **(d–f)** The densities of total spines (**d**), stubby spines (**e**), and mushroom spines (**f**) were downregulated in the STZ group compared with vehicle mice (****p < 0.0001 **(d)**, **p = 0.0078 **(e)**, ****p < 0.0001 **(f)** between vehicle and STZ), which all rescued after exercise (n = 20/group) (***p = 0.0003 **(d)**, **p = 0.0078 **(e)**, **p = 0.0026 **(f)** between STZ and STZ + Run). **(g)** Representative images of dendritic spine 3D reconstruction to classify stubby, mushroom, long thin, and filopodia spines. Scale bar, 5 μm. **(h–i)** Representative immunoblots of synaptic proteins: PSD95 (**h**) and SYP (i) (n = 6/group) (*p = 0.0118 **(h)**, *p = 0.0291 **(i)** between vehicle and STZ) (*p = 0.0209 **(h)**, *p = 0.0345 **(i)** between STZ and STZ + Run). **(j)** Representative images of mEPSC traces in CA1 pyramidal neurons. **(k, m)** Average neuron mEPSC frequency (**k**) and amplitude (**m**) (n = 9/group) (***p = 0.0002 between vehicle and STZ, *p = 0.0159 between STZ and STZ + Run). **(l, n)** Cumulative distributions of mEPSC frequency (**l**) and amplitude (**n**) (n = 9/group). Data are presented as mean ± SEM. One-way ANOVA with Tukey's multiple comparisons test was performed in **c–f, h–i, k**.

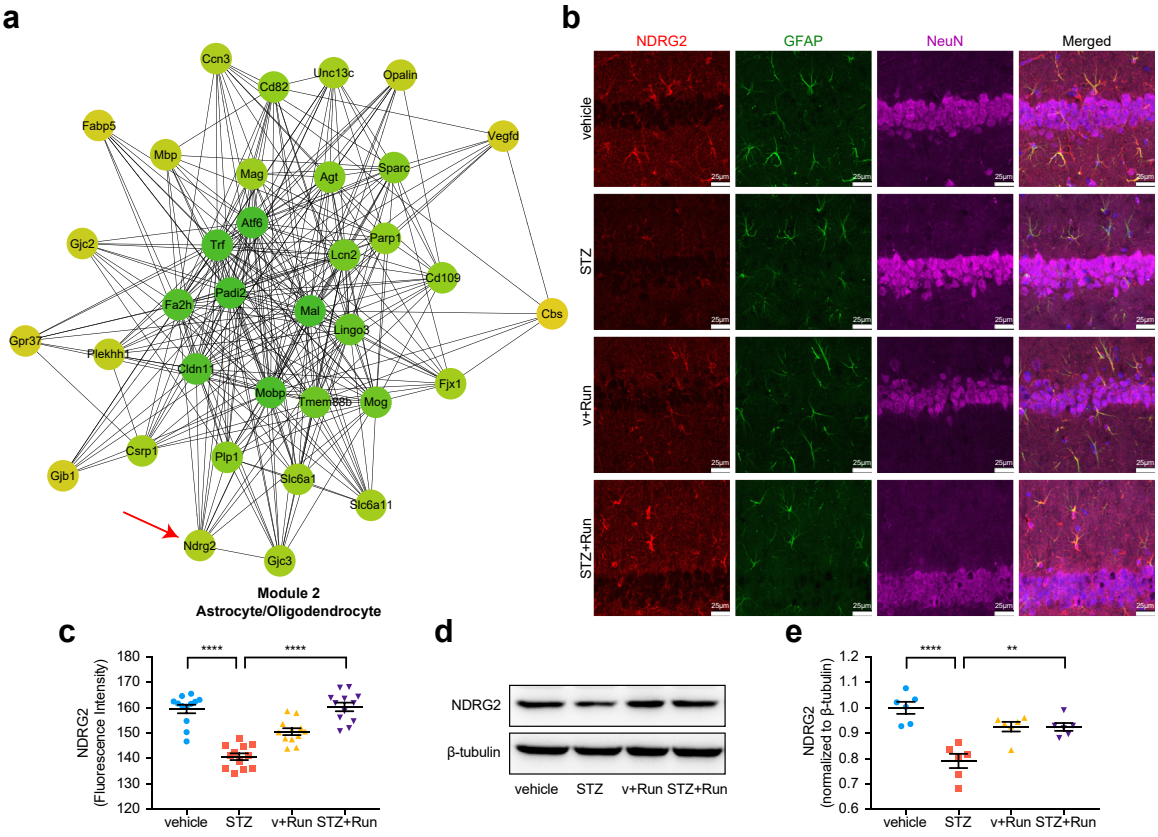

Fig. 3: **Exercise reverses the downregulation of astrocytic NDRG2 in the diabetic hippocampus. (a)** Astrocytic and oligodendrocytic genes (Ndrg2, Lcn2, and Mobp) were enriched in module 2. **(b–c)** Representative immunofluorescent staining of NDRG2 in the hippocampus **(b);** the fluorescent intensity **(c)** was decreased at STZ group compared with vehicle mice (****p < 0.0001 between vehicle and STZ), which was upregulated by exercise (****p < 0.0001 between STZ and STZ + Run). Red: NDRG2, green: GFAP, purple: NeuN. Scale bar, 25 μm. **(d–e)** Representative immunoblots of astrocytic NDRG2 in the hippocampus exhibited downregulated at STZ mice compared with vehicle (****p < 0.0001 between vehicle and STZ), which was increased after exercise (n = 6/group) (**p = 0.0018 between STZ and STZ + Run). Data are presented as mean ± SEM. One-way ANOVA with Tukey's multiple comparisons test was performed in **c, e**.

protein levels were normalized after NDRG2 overexpression in the STZ + AAV-NDRG2 group (Fig. 5k–n). The automatic classification of dendritic spine density demonstrated that overexpression of NDRG2 reversed the reductions in stubby, mushroom, and total spine densities in diabetic mice but did not significantly impact long thin or filopodia spine density (Fig. 5o and p and Fig. S4a–d). Above all, these findings indicate that NDRG2 overexpression protects diabetic mice from dendritic spine loss and cognitive defects.

Astrocytic NDRG2 restores neuronal synaptic plasticity in diabetic mice via inhibiting NF-κB/C3 signaling

Astrocytic inflammatory response genes were enriched in module 17, characterized by containing the most abundant genes in transcriptomic WGCNA (Fig. S2d). Hub genes related to complement activation of microglia —*Klf17*, *C1s2*, and *F3*— were enriched in module 8, whereas genes associated with complement and coagulation cascades, including *Fga, F9, Cxcr2, and Fgg*, were enriched in module 11 (Fig. S2b and c). Interestingly, we identified positive correlations among module 17, module 8, and module 11 (Fig. 1k), which reflects the biological mechanisms that complement activation of microglia, astrocyte inflammatory response, and complement and coagulation cascades are intimately linked to each other.

To validate the correlation network of RNA-sequencing, we analyzed the results of TMT-labeled proteomic sequencing of the hippocampus tissue in the vehicle, STZ, and STZ + Run mice. PCA analysis illustrated that the distribution of samples was discrete among groups and concentrated within each group (Fig. S3a). The threshold used for differentially expressed proteins were fold-changes >1.2 or <0.83, accompanied by a p-value <0.05. A total of 151 upregulated proteins and 29 downregulated proteins were

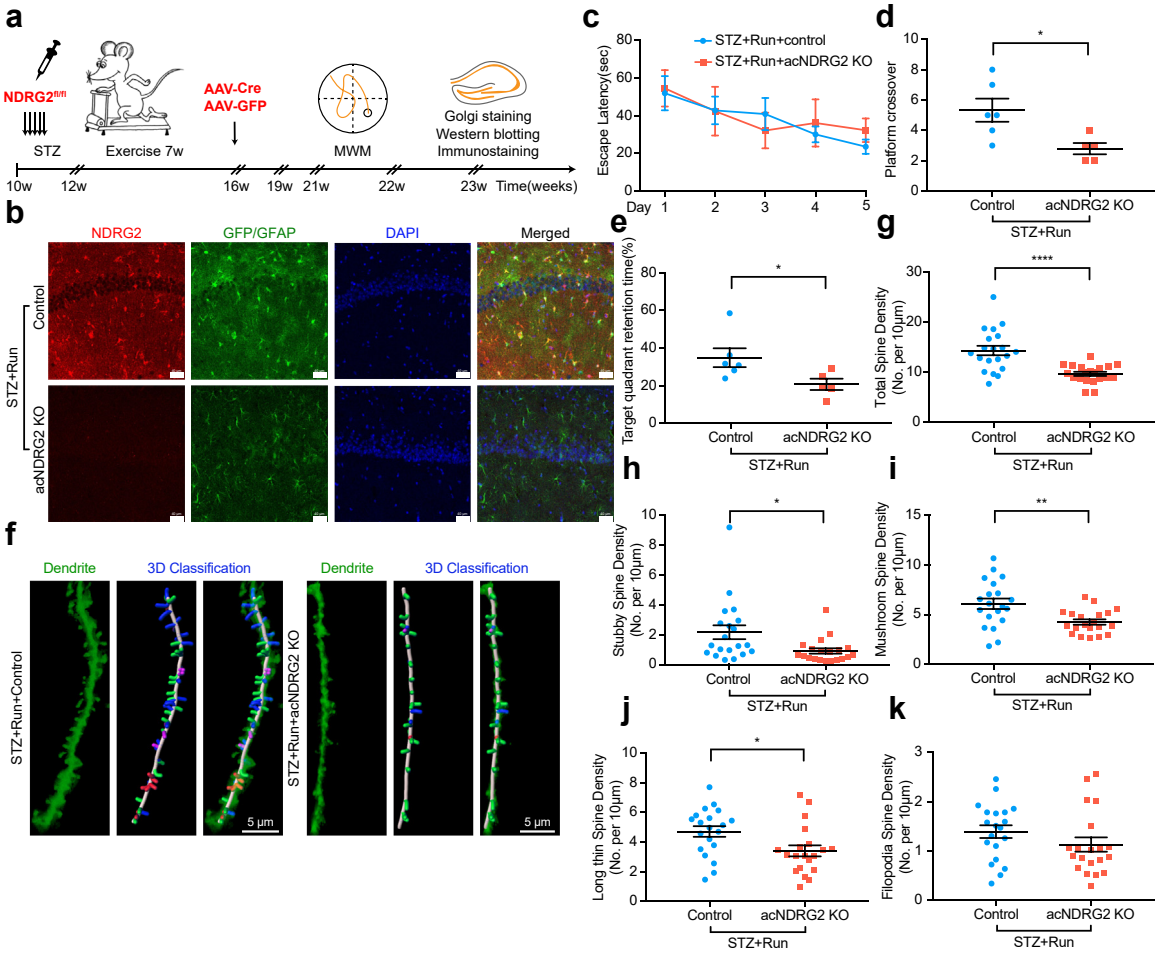

Fig. 4: **NDRG2 deficiency reverses the beneficial effect of exercise on the dendritic spine and cognitive function in diabetic mice. (a)** Schematic representing chronological order of STZ injection, exercise, AAV-Cre to induce NDRG2 deficiency, and behavioral testing. **(b)** Representative microscopic fields of NDRG2 deficiency in the hippocampus. Red: NDRG2, green: GFP/GFAP, blue: DAPI. Scale bar, 40 μm. (**c**) The escape latency of MWM tests. **(d–e)** The platform crossover (**d**) and target quadrant retention time (%) (**e**) of MWM tests were decreased in the STZ + Run + acNDRG2 KO group (n = 5) compared with STZ + Run + control mice (n = 6) (*p = 0.0208 **(d)**, *p = 0.0477 **(e)** between STZ + Run + acNDRG2 KO and STZ + Run + control). **(f)** Representative images of dendritic spine 3D reconstruction in the STZ + Run + acNDRG2 KO and STZ + Run + control mice. Scale bar, 5 μm. **(g–j)** The densities of total spines (**g**), stubby spines (**h**), mushroom spines (**i**), and long thin spines (**j**) were downregulated in the STZ + Run + acNDRG2 KO group compared with STZ + Run + control mice (n = 20/group) (****p < 0.0001 **(g)**, *p = 0.0164 **(h)**, **p = 0.0035 **(i),** *p = 0.0153 **(j)** between STZ + Run + acNDRG2 KO and STZ + Run + control). (**k**) The densities of filopodia spines (n = 20/group). Data are presented as mean ± SEM. Two-tailed Student's t-test was performed in **d–j**.

detected in diabetic mice, whereas a volcano plot showed six upregulated proteins and 78 downregulated proteins in STZ + Run mice (Fig. S3b–d). The results of proteomic GSEA were consistent with correlation network analysis of RNA-sequencing, which involves complement coagulation cascades and long-term potentiation pathways. The complement and coagulation cascades were enriched at the top of the ranked list in STZ mice compared to vehicle mice (p = 0.0002, STZ vs. vehicle, NES = 2.22). Furthermore, these cascades concentrated at the bottom of the list in STZ + Run mice (p = 0.0035, STZ + Run vs. STZ, NES = –1.82). Overall, these findings reflect the upregulation of complement and coagulation cascades in diabetic mice and subsequent downregulation following exercise (Fig. 6a). The long-term potentiation pathways were enriched at the bottom of the ranked list in diabetic mice (p = 0.0445, STZ vs. vehicle, NES = –1.40), and at the top of the list in the STZ + Run group (p = 0.0041, STZ + Run vs. STZ, NES = 1.69). These findings are consistent with WGCNA analysis, which showed that injury in neuronal synaptic plasticity occurred in diabetic mice and was reversed after exercise (Fig. S3e). The expression levels of C3, FGA, FGG, and FGB proteins involved in

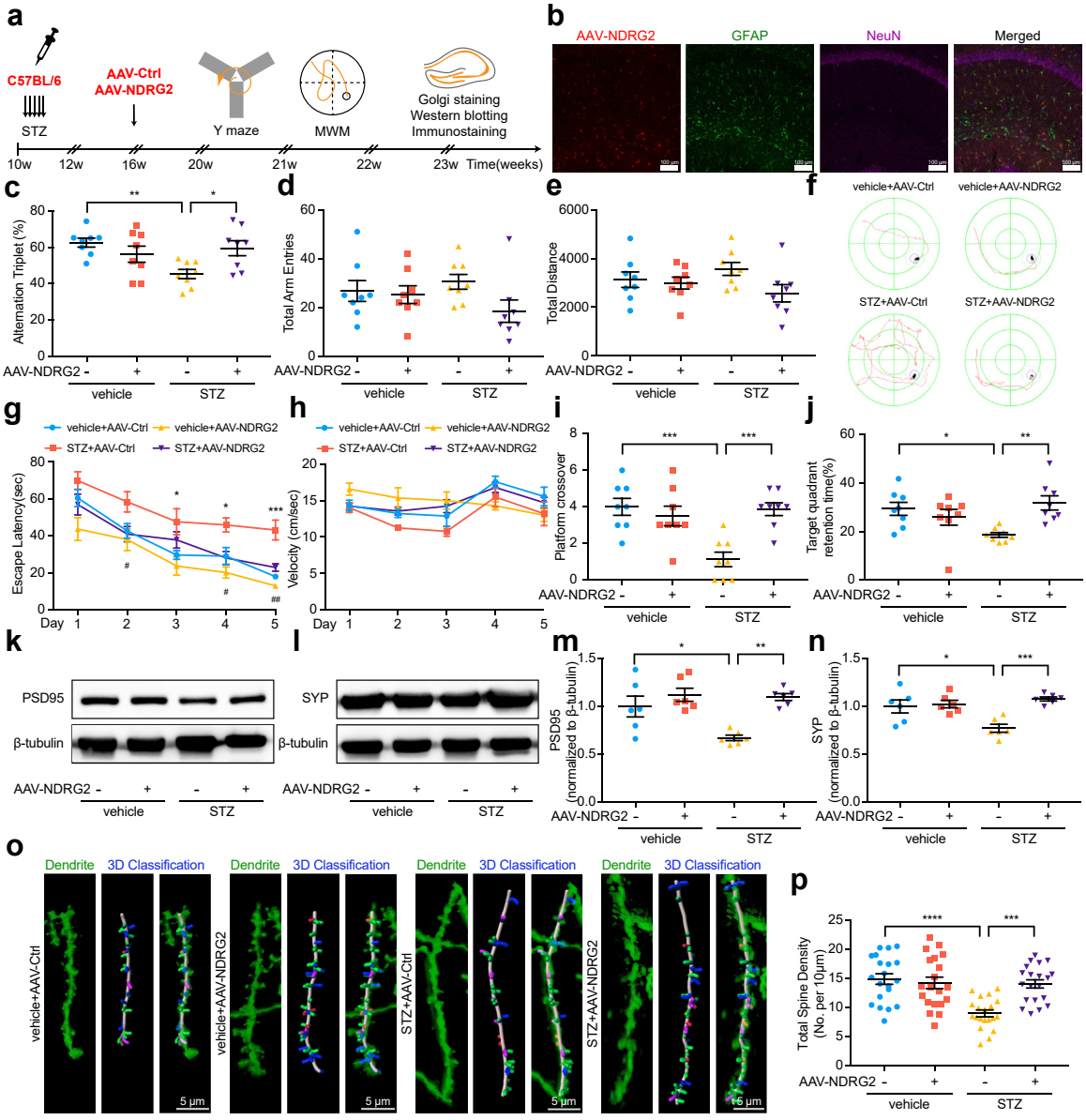

Fig. 5: **NDRG2 overexpression alleviates synaptic injury and memory deficits at diabetic mice.** **(a)** Schematic representing chronological order of STZ injection, NDRG2 overexpression, and behavioral testing. **(b)** Representative immunofluorescent staining of NDRG2 overexpression in the hippocampus. Red: NDRG2, green: GFAP, purple: NeuN, blue: DAPI. Scale bar, 100 μm. **(c)** Y-maze alternation triplet (%) were increased at the STZ + AAV-NDRG2 group compared to STZ + AAV-Ctrl group (n = 8/group) (**p = 0.0082 between vehicle + AAV-Ctrl and STZ + AAV-Ctrl) (*p = 0.0368 between STZ + AAV-NDRG2 and STZ + AAV-Ctrl). **(d–e)** Y-maze total arm entries (**d**) and total distance (**e**) (n = 8/group). **(f)** Representative traces of diabetic or non-diabetic mice after NDRG2 overexpression from the MWM test. **(g)** Escape latency was reduced at the STZ + AAV-NDRG2 mice compared to STZ + AAV-Ctrl group (n = 8/group) (*p = 0.0279 **(day 3)**, *p = 0.0456 **(day 4)**, ***p = 0.0007 **(day 5)** between vehicle + AAV-Ctrl and STZ + AAV-Ctrl) ($^{\#}p$ = 0.0341 **(day 2)**, $^{\#}p$ = 0.0297 **(day 4)**, $^{\#\#}p$ = 0.0100 **(day 5)** between STZ + AAV-NDRG2 and STZ + AAV-Ctrl). **(h)** Swimming velocity during the MWM test (n = 8/group). **(i–j)** The platform crossover (**i**) and target quadrant retention time (%) (**j**) during the probe trial of the MWM test were increased after NDRG2 overexpression (n = 8/group) (***p = 0.0005 (**i**), *p = 0.0331(**j**) between vehicle + AAV-Ctrl and STZ + AAV-Ctrl) (***p = 0.0007 **(i)**, **p = 0.0067 **(j)** between STZ + AAV-NDRG2 and STZ + AAV-Ctrl). **(k–n)** Representative immunoblots of synaptic proteins: PSD95 (**k, m**) and SYP (**l, n**), the protein levels improved in the STZ + AAV-NDRG2 group compared to STZ + AAV-Ctrl mice (n = 6/group) (*p = 0.0138 (**m**), *p = 0.010 (**n**) between vehicle + AAV-Ctrl and STZ + AAV-Ctrl) (**p = 0.0014 **(m)**, ***p = 0.0006 **(n)** between STZ + AAV-NDRG2 and STZ + AAV-Ctrl). **(o)** Representative images of 3D reconstruction of dendritic spines. Scale bar, 5 μm. **(p)** The densities of total spines were upregulated at the STZ + AAV-NDRG2 group compared to STZ + AAV-Ctrl mice (n = 20/

complement and coagulation cascades and proteins involved in long-term potentiation pathways are illustrated in the heat map (Fig. 6b and Fig. S3f).

As a key node in complement cascades, we verified the expressions of complement C3. The immunofluorescence intensities of C3 were increased in STZ groups compared with vehicle mice, which were restored by exercise (Fig. 6c and d). Meanwhile, we also found that C3 protein levels were increased in diabetic mice and decreased following exercise (Fig. 6e and f), suggesting that astrocytes were activated into their neurotoxic A1 form in diabetic mice and attenuated after exercise. More importantly, the expression levels of C3 and p-NF-κB were increased in STZ + Run + acNDRG2 KO mice compared to STZ + Run + control mice (Fig. 6g–k), which indicates that NDRG2 depletion promoted abnormal NF-κB activation, and complement C3, as an astrocytic target of NF-κB signaling, was aberrantly released, thus impaired dendritic spines and cognitive function in diabetic mice.

Although we confirmed that complement C3 levels were increased in diabetic mice and more seriously elevated after astrocytic NDRG2 loss-of-function, we sought to find a better intervention to reduce the production of C3 at its source. We attempted overexpression of NDRG2 in primary astrocytes *in vitro* (Fig. S4e–g). After treatment with high glucose, the content of complement C3 was increased, and expression of NDRG2 was decreased in primary astrocytes (Fig. S4h–j). Overexpression of NDRG2 could inhibit the higher levels of complement C3 and improves neuron survival (Fig. S4h–l). We transfected LV-shRNA-NDRG2 to downregulate NDRG2, and applied NF-κB inhibitors: BAY11–7082 in primary astrocyte. We observed that the deficiency of NDRG2 failed to induce the activation of complement C3 in the presence of NF-κB inhibitors (Fig. S4m and n), which indicated the NDRG2/NF-κB/C3 signal pathway.

Then, we also investigated whether NDRG2 overexpression included a remodeling of the pathological structure of astrocytes to inhibit the production of C3 in diabetic mice. Consistent with our previous results, the levels of NDRG2 were decreased in the STZ + AAV-Ctrl group compared to those in the vehicle + AAV-Ctrl group, further verified the downregulation of NDRG2 in diabetic mice. The levels of NDRG2 were overexpressed in both vehicle + AAV-NDRG2 and STZ + AAV-NDRG2 groups. The overexpression of NDRG2 restored the heightened levels of p-NF-κB and C3 in diabetic mice (Fig. 6l–n), indicating that a gain-of-function in NDRG2 could inhibit complement signaling and neurotoxic characteristic.

C3aR antagonist rescues dendritic spine loss and cognitive dysfunction in diabetic mice

We illustrated that abnormally high C3 levels induced synaptic injury of neighboring neurons in diabetic mice. Then, we used C3aR antagonists to clarify whether C3aR blockade could mimic the protective effect of NDRG2 overexpression on DACD and rescue dendritic spine loss and cognitive deficits in diabetic mice (Fig. 7a). The Y-maze alternation triplet (%) was decreased in STZ + PBS mice compared to vehicle + PBS mice, while C3aR blockade improved the alternation triplet (%) in the STZ + C3aRA group (Fig. 7b). There were no significant differences in total arm entries or total distance between each group (Fig. 7c and d). In the MWM tests, the C3aR antagonist was found to reverse both delayed escape latency and lower platform crossover in the STZ + C3aRA group compared to STZ + PBS mice (Fig. 7e and f). Automatic classification of dendritic spines proved that C3aR blockade reverses the reduction of total spine density, particularly regarding mushroom and stubby spines, in STZ + C3aRA mice compared to the STZ + PBS groups (Fig. 7g–l). Taken together, these results indicate that C3aR antagonist treatment could mimic the protective effect of NDRG2 overexpression, rescue cognitive impairment and restore synaptic refinement in diabetic mice.

Complement C3 may be a predictor for cognitive dysfunction in diabetic patients

In mice with diabetes-associated cognitive dysfunction, we observed significantly increased levels of C3 in the hippocampus, which induced synaptic spine loss and cognitive deficits. As an extension of these results, differences in cognitive function between diabetic and normal patients were assessed. We collected the serum and metabolic indicators from thirteen non-diabetic and twenty-seven diabetic patients, then assessed cognitive function using the Digit Symbol Substitution Test (DSST) scoring system. No differences were observed between the two groups regarding baseline clinical data (Table 1), such as age (66.69 ± 1.168 y in non-diabetic and 68.96 ± 0.9526 y in diabetic patients), BMI (22.99 ± 0.5683 in non-diabetic and 24.08 ± 0.4765 in diabetic patients), systolic blood pressure, and diastolic blood pressure (Fig. S5a–d). However, the average DSST score of diabetic patients (22.04 ± 1.783) was significantly lower than that of non-diabetic peers (38.31 ± 2.305) (Fig. 7m). Although given standard glycemic control, the fasting plasma glucose of diabetic patients (6.889 ± 0.3237 mmol/L) was higher than that of non-diabetic patients (4.618 ± 0.3234 mmol/L)

group) (****$p < 0.0001$ between vehicle + AAV-Ctrl and STZ + AAV-Ctrl) (***$p = 0.0002$ between STZ + AAV-NDRG2 and STZ + AAV-Ctrl). Data are presented as mean ± SEM. One-way ANOVA with Tukey's multiple comparisons test was performed in **c, i–p**. Two-way ANOVA with Tukey's multiple comparisons test was performed in **g**.

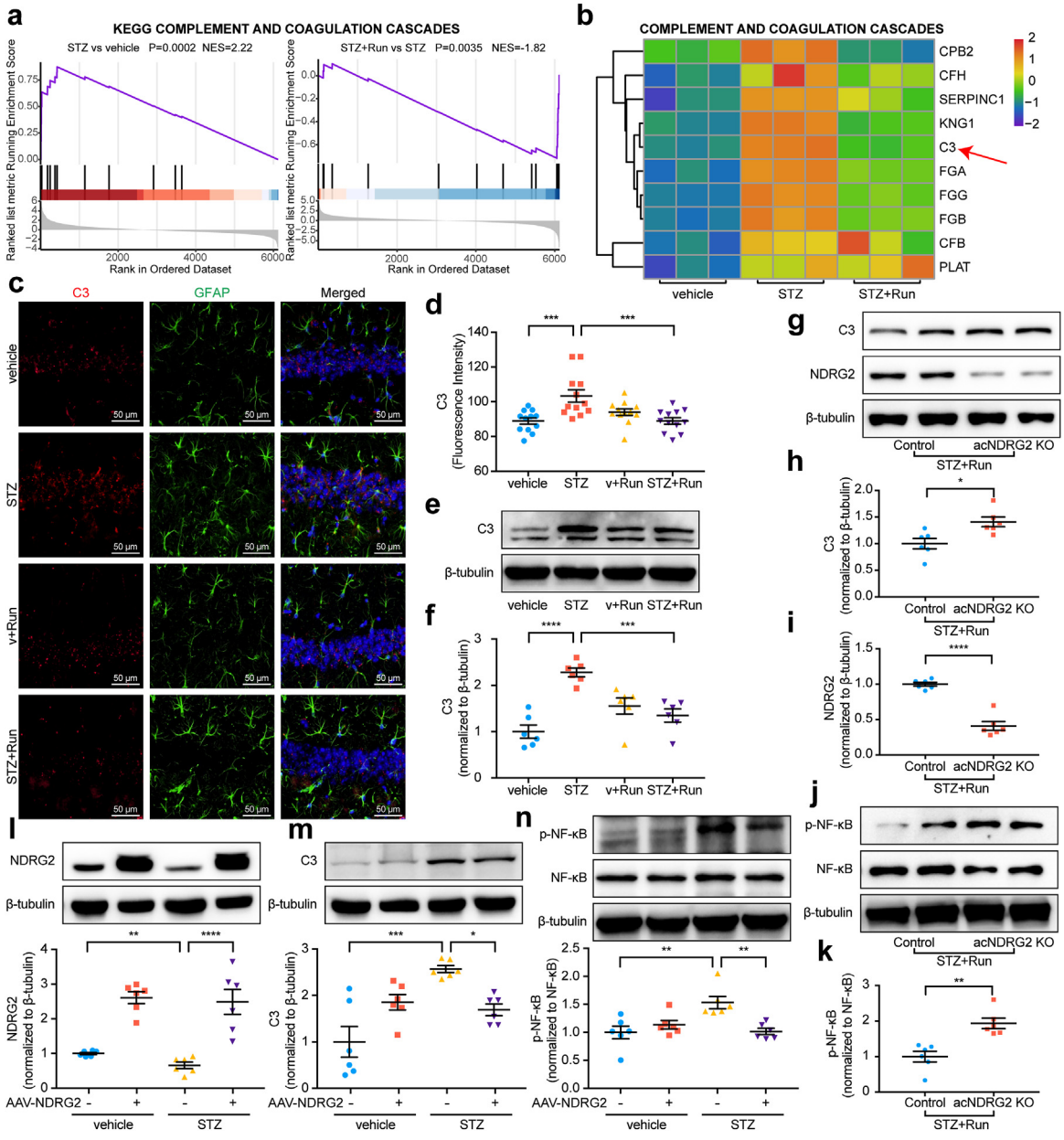

Fig. 6: **NDRG2 reshapes the pathological structure of astrocytes by inhibiting NF-κB/C3 signaling. (a)** GSEA of proteome indicated complement and coagulation cascade signaling were upregulated in diabetic mice (***p = 0.0002 between vehicle and STZ) and downregulated after exercise (**p = 0.0035 between STZ and STZ + Run). The cumulative enrichment scores were normalized (NES) (n = 3/group). **(b)** Heatmaps showing the fold changes of significantly altered proteins in complement and coagulation cascades (n = 3/group). **(c–d)** Representative immunofluorescent staining of intact C3 and its cleaved products in the hippocampus. Red: C3, green: GFAP, blue: DAPI. Scale bar, 50 μm. (***p = 0.0006 between vehicle and STZ, ***p = 0.0006 between STZ and STZ + Run) **(e–f)** Representative immunoblots of complement C3 in the hippocampus were increased in the STZ group compared to vehicle mice (****p < 0.0001 between vehicle and STZ), which was downregulated after exercise (n = 6/group) (***p = 0.0008 between STZ and STZ + Run). **(g–k)** Representative immunoblots of astrocytic NDRG2 (**g, i**), complement C3 (**g, h**), NF-κB, and p-NF-κB (**j, k**) after NDRG2 loss of function (n = 6/group) (*p = 0.0120 **(h)**, ****p < 0.0001 **(i)**, **p = 0.0012 **(k)** between STZ + Run + acNDRG2 KO and STZ + Run + control). **(l–n)** Representative immunoblots of astrocytic NDRG2 (**l**), complement C3 (**m**), NF-κB, and p-NF-κB (**n**) in the hippocampus after NDRG2 gain of function (n = 6/group) (**p = 0.0064 (**l**), ***p = 0.0001 (**m**), **p = 0.0029 (**n**) between vehicle + AAV-Ctrl and STZ + AAV-Ctrl) (****p < 0.0001 (**l**), *p = 0.0264 **(m)**, **p = 0.0040 **(n)** between STZ + AAV-NDRG2 and STZ + AAV-Ctrl). Data are presented as mean ± SEM. GSEA analysis was performed in **a**. One-way ANOVA with Tukey's multiple comparisons test was performed in **d, f, l–n**. Two-tailed Student's t-test was performed in **h, i, k**.

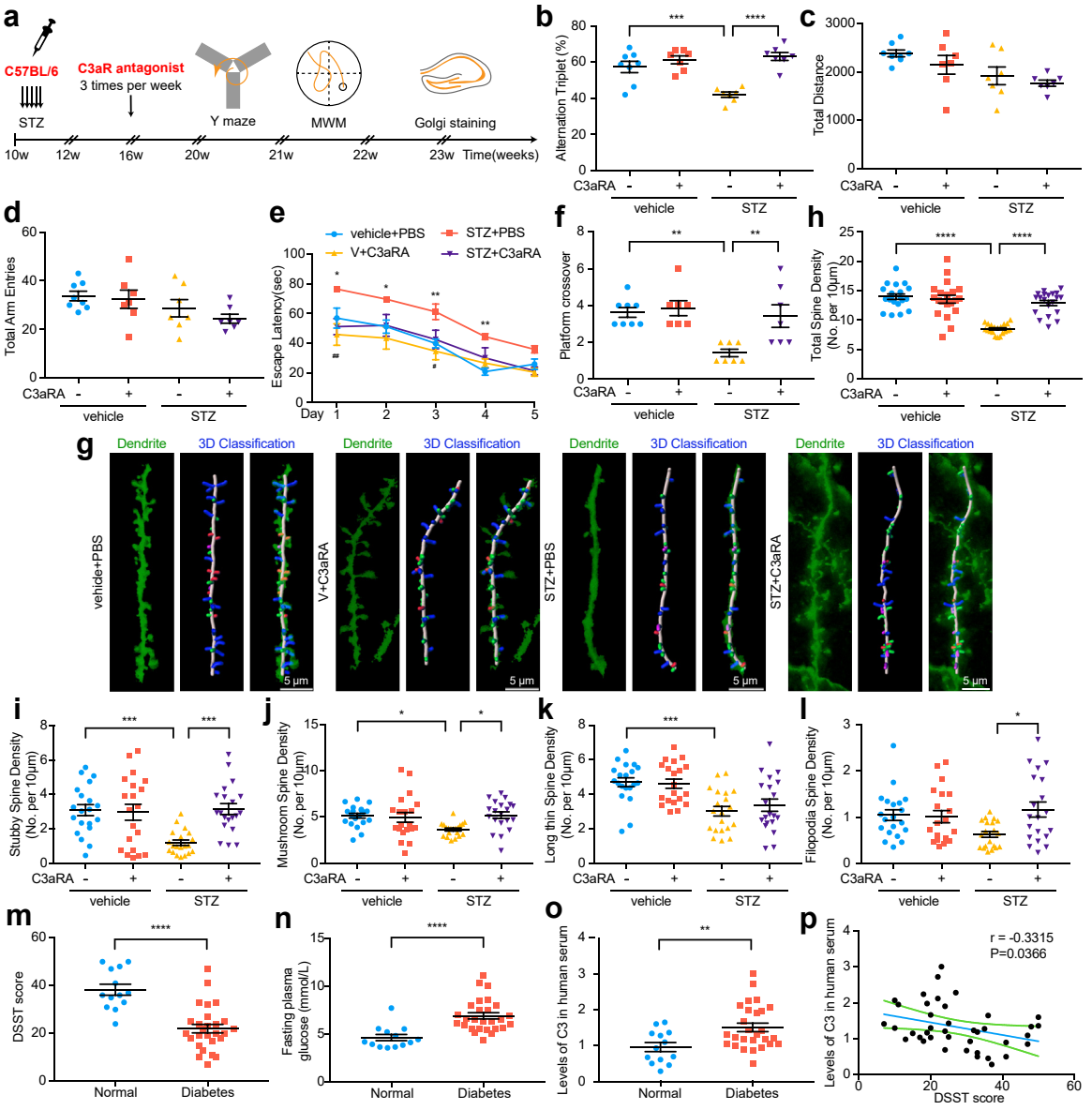

Fig. 7*: C3aR blockade rescues dendritic spine loss in diabetic mice, and C3 may be a biomarker to predict the progression of DACD in humans. (a)** Schematic representing chronological order of STZ injection, C3aR antagonist, and behavioral testing. We used C3aR antagonists to clarify whether C3aR blockade could mimic the protective effect of NDRG2 overexpression on DACD. **(b)** Y-maze alternation triplet (%) was improved in the STZ + C3aRA group compared with STZ + PBS mice (n = 7/group, n = 8 vehicle + PBS) (p = 0.0006 between vehicle + PBS and STZ + PBS) (****p < 0.0001 between STZ + C3aRA and STZ + PBS). **(c–d)** Y-maze total distance (**c**) and total arm entries (**d**) (n = 7/group, n = 8 vehicle + PBS). **(e)** Escape latency of MWM test was shorten at the STZ + C3aRA group compared with STZ + PBS mice (n = 7/group, n = 8 vehicle + PBS) (*p = 0.0211 **(day 1)**, *p = 0.0336 **(day 2)**, **p = 0.0099 **(day 3)**, **p = 0.0033 **(day 4)** between vehicle + PBS and STZ + PBS) ($^{\#\#}p$ = 0.0021 **(day 1)**, $^{\#}p$ = 0.0392 **(day 3)** between STZ + C3aRA and STZ + PBS). **(f)** Platform crossover of MWM test was upregulated at the STZ + C3aRA mice compared to STZ + PBS group (n = 7/group, n = 8 vehicle + PBS) (**p = 0.0025 between vehicle + PBS and STZ + PBS) (**p = 0.0066 between STZ + C3aRA and STZ + PBS). **(g)** Representative images of 3D reconstruction of dendritic spines. Scale bar, 5 μm. **(h–l)** The densities of total spines (**h**), stubby spines (**i**), mushroom spines (**j**), long thin spines (**k**), and filopodia spines (**l**) (n = 20/group) (****p < 0.0001 (**h**), ***p = 0.0008 (**i**), *p = 0.0191 (**j**), ***p = 0.0006 (**k**) between vehicle + PBS and STZ + PBS) (****p < 0.0001 (**h**), ***p = 0.0005 (**i**), *p = 0.0133 (**j**), *p = 0.0153 (**l**) between STZ + C3aRA and STZ + PBS). **(m)** The DSST scores of diabetic patients (n = 27) and non-diabetic peers (n = 13) (****p < 0.0001 between Normal and Diabetes). **(n)** Fasting plasma glucose levels for diabetic patients (n = 27) compared to non-diabetic patients (n = 13) (****p < 0.0001 between Normal and Diabetes). **(o)** The serum levels of complement C3 in diabetic patients (n = 27) and normal peers (n = 13) (**p = 0.0072 between Normal and Diabetes). **(p)** The correlations between DSST score and

(Fig. 7n). Additionally, the insulin resistance index HOMA-IR of diabetic patients was 1.803 times higher than that of non-diabetic patients (Fig. S5e). We found that the DSST score was negatively correlated with fasting plasma glucose (r = –0.4356, p = 0.0050) and HOMA-IR value (r = –0.3469, p = 0.0283) by performing univariable logistic regression (Fig. S5f and g). More importantly, levels of complement C3 in human serum were elevated in diabetic patients (1.506 ± 0.1185 mg/mL) compared to those in non-diabetic patients (0.9587 ± 0.1268 mg/mL) (Fig. 7o). Cognitive DSST score was negatively correlated with C3 level by performing univariable logistic regression (r = –0.3315, p = 0.0366) (Fig. 7p). Furthermore, a multivariate logistic regression analysis was performed. The DSST score was only correlated with groups (R^2 = 0.417, F = 28.851, p < 0.0001) (Tables 2–4), which verified that DSST scores were significantly lower in diabetes than non-diabetes. Risk factors, such as C3, fasting plasma glucose (FPG), and HOMA-IR value were considered potential confounders in the multivariate logistic regression analysis (Table 5). Our results suggest that serum C3 levels might be associated with cognitive deficits in diabetic patients.

Variable	Non-diabetic patients (n = 13)	Diabetic patients (n = 27)	P value
Age, years	66.69 ± 1.168	68.96 ± 0.9526	0.1631
Sex (Male, %)	76.92%	62.96%	–
Height(m)	1.662 ± 0.01713	1.66 ± 0.01749	0.9564
Weight (kg)	63.69 ± 2.333	66.48 ± 1.918	0.3901
BMI, kg/m^2	22.99 ± 0.5683	24.08 ± 0.4765	0.1785
SBP, mmHg	129.5 ± 5.214	136.1 ± 4.275	0.3615
DBP, mmHg	77.23 ± 3.606	81.3 ± 1.754	0.2585
C3, mg/mL	0.9587 ± 0.1268	1.506 ± 0.1185	0.0072
DSST score	38.31 ± 2.305	22.04 ± 1.783	<0.0001
FPG, mmol/L	4.618 ± 0.3234	6.889 ± 0.3237	<0.0001
Insulin, mIU/L	0.8802 (0.7803–1.226)	1.065 (0.8341–1.441)	0.1889
HOMA-IR	1 ± 0.1102	1.803 ± 0.1529	0.0015

Data are expressed as mean SEM, median (interquartile range). SBP: Systolic blood pressure; DBP: Diastolic blood pressure; FPG: Fasting plasma glucose; Insulin: Fasting insulin, mIU/L.

Table 1: **Characteristics of the study population.**

Model summary[b]

Model	R	R square	Adjusted R square	Std. error of the estimate	Durbin–Watson
1	0.657[a]	0.432	0.417	8.973	0.320

[a]Predictors: (Constant), Group. [b]Dependent Variable: DSST.

Table 2: **Model summary of multivariate logistic regression analyses.**

ANOVA[a]

Model		Sum of squares	df	Mean square	F	Sig.
1	Regression	2323.043	1	2323.043	28.851	0.000[b]
	Residual	3059.732	38	80.519		
	Total	5382.775	39			

[a]Dependent Variable: DSST. [b]Predictors: (Constant), Group.

Table 3: **ANOVA of multivariate logistic regression analyses.**

Discussion

In this study, we analyzed the integrative pathogenesis of DACD by conducting transcriptomic and TMT quantitative proteomic sequencing of hippocampal tissue from diabetic mice, which revealed that the activation of complement cascades accelerates the impairment of neuronal synaptic plasticity. In addition, we discovered that NDRG2 acts as a regulator of astrocytic-neuronal interaction via NF-κB/C3/C3aR signaling to restore synaptic function in diabetic mice.

We performed WGCNA of the transcriptome and classified 18 modules in a cluster dendrogram. Module 1 was enriched in genes related to neuronal synaptic plasticity, module 2 was enriched in Ndrg2 and Lcn2 genes related to astrocytes, modules 4 & 17 were enriched in the endoplasmic reticulum and astrocytic inflammatory response genes, and modules 8 & 11 were enriched in complement cascade genes. We then determined the relationships between each module, identifying a highly negative correlation between module 1, module 2, and module 4, which reflected the negative relationship between astrocytic inflammatory response and neuronal synaptic plasticity in diabetic mice. Consistent with our results, WGCNA from a large proteomic study on the AD brain and cerebrospinal fluid demonstrated that AD pathology and cognitive dysfunction were correlated with proteins linked to astrocytic and microglial activation.[45] We also identified positive correlations among module 17, module 8, and module 11, which suggested that activated microglia promote astrocytes to secrete large amounts of C3, amplifying complement cascades and immune inflammation and ultimately leading to impairment of synaptic plasticity. It had been reported that microglia-derived C1q, TNFα, and Il-1α work together to induce A1 reactive astrocytes.[46] A1 reactive astrocytes characteristically upregulate the expression of astrocytic C3 to initiate complement and coagulation cascades. Then, astrocytes

increased C3 levels in diabetic patients (n = 27) and normal peers (n = 13). Correlations were found using linear regression, with r = –0.3315 and p = 0.0366. Values presented as mean ± SEM. Two-way ANOVA with Tukey's multiple comparisons test was performed in **e**. One-way ANOVA with Tukey's multiple comparisons test was performed in **b, f–l**. Two-tailed Student's t-test was performed in **m–o**.

Coefficients[a]

Model		Unstandardized	Coefficients	Standardized coefficients	t	Collinearity statistics		
		B	Std. error	Beta		Sig.	Tolerance	VIF
1	Constant	54.578	5.269		10.359	0.000		
	Group	−16.271	3.029	−0.657	−5.371	0.000	1.000	1.000

[a]Dependent Variable: DSST.

Table 4: **Coefficients of multivariate logistic regression analyses.**

Excluded variables[a]

Model		Beta In	t	Sig.	Partial correlation	Collinearity statistics		
						Tolerance	VIF	Minimum tolerance
1	Age	−0.142[b]	−1.139	0.262	−0.184	0.949	1.053	0.949
	BMI	−0.090[b]	−0.711	0.481	−0.116	0.953	1.049	0.953
	SBP	−0.124[b]	−1.000	0.324	−0.162	0.978	1.022	0.978
	DBP	0.048[b]	0.383	0.704	0.063	0.967	1.035	0.967
	Glucose	−0.083[b]	−0.551	0.585	−0.090	0.665	1.504	0.665
	C3	−0.069[b]	−0.504	0.617	−0.083	0.825	1.213	0.825
	HOMAIR	−0.036[b]	−0.255	0.800	−0.042	0.764	1.309	0.764
	Insulin	−0.017[b]	−0.134	0.894	−0.022	0.949	1.054	0.949

[a]Dependent Variable: DSST. [b]Predictors in the Model: (Constant), Group.

Table 5: **Excluded variables of multivariate logistic regression analyses.**

lose their protective function of promoting synaptic formation and acquire strong neurotoxicity, thus injuring neuronal synaptic plasticity.[47,48] In neurodegenerative diseases, C3 has strong neurotoxic properties and mediates the overactivation of the complement cascade, which damages synaptic structures and matured oligodendrocytes.

Furthermore, GSEA of proteomic sequencing results demonstrated that the complement cascade pathway was overactivated in diabetic mice, and it was accompanied by significant upregulation of complement C3 and downregulation of long-term potentiation-related proteins, such as those within the MAPK and CaMK families. From a microscopic perspective, we classified the 3D structures of dendritic spines and induced miniature excitatory postsynaptic currents (mEPSCs) to observe synaptic transmission, which all illustrated impairment of neuronal synaptic plasticity. Furthermore, the secretion of C3, which impairs neuronal synaptic plasticity and memory loss,[49] was assessed. We found that C3 levels were significantly increased in diabetic mice and decreased after exercise. Moreover, the expression levels of NDRG2, PSD95, and SYP were significantly decreased in diabetic mice, and these deficits were reversed by exercise. To sum up, this data revealed that astrocytic NDRG2/C3 has a vital role in neuronal synaptic plasticity.

Astrocytes are the primary secretory source of C3[28], and NDRG2 is specifically expressed in astrocytes.[50] The deficiency of NDRG2 is closely related to the pathogenesis of attention-deficit/hyperactivity disorder and memory impairment[14] and can aggravate cerebral ischemic injury and cognitive impairment in AD.[21] Additionally, previous research has shown that loss of NDRG2 altered astrocytic morphology and neuronal communication by regulating the accumulation of the Rho-GTPase pathway.[51] Furthermore, deletions of the 14q11.2 chromosome, which encodes NDRG2 genes that associated with neurite outgrowth, was reported in three children and resulted in developmental delay, cognitive impairment, and facial anomalies.[52] Previous studies revealed that NDRG2 overexpression act as an anti-tumor role through inhibiting NF-κB, STAT3 and TGF-β-mediated cell signaling.[53,54] To further explore whether NDRG2 is involved in the activation of complement cascades and synaptic injury, we performed conditional astrocytic NDRG2 knockout in STZ + Run mice. The deficiency of NDRG2 promoted phosphorylation of NF-κB and induced abnormal NF-κB activation, thus accelerating the expression of C3 and complement cascades and ultimately leading to dendritic spine loss and cognitive dysfunction. This result demonstrated that NDRG2 deficiency reversed the protective effect of exercise and aggravates dendritic spine loss and cognitive dysfunction in diabetic mice via NF-κB and C3 signaling. It has been reported that the complement C3 promoter includes two NF-κB binding sites and that direct binding of NF-κB to the C3 promoter can initiate transcription of C3, as validated by chromatin immunoprecipitation.[29] Thus, C3 was significantly increased at the astrocyte-specific IκBα (inhibitor kappa B alpha, an inhibitor of NF-κB) deletion mice.[29] This finding further confirmed that C3 acts as a direct NF-κB target within astrocytes.[29] Furthermore, we found that the overexpression of NDRG2 could promote the remodeling of neurotoxic astrocytes by inhibiting p-NF-κB and C3 signaling. In addition, NDRG2 overexpression increased the expression of synaptic proteins PSD95 & SYP and dendritic spine density, thus attenuating synaptic injury and cognitive deficits in diabetic mice. Moreover, overexpression of NDRG2 could inhibit the higher levels of complement C3 in primary astrocytes *in vitro*, and NDRG2 deficiency failed to induce the activation of complement C3 in the presence of NF-κB inhibitors. These results confirm that the expression of NDRG2 is closely related to the cognitive function of diabetic mice, which regulates the activation of complement cascades by inhibiting p-NF-κB.

In aging and neurodegenerative diseases, microglia and astrocytes have been found to be the main sources of secreting complement components, while neurons, endothelial cells, and oligodendrocytes act as additional contributors. Furthermore, C3aR is expressed in

neurons, vascular endothelial cells, and microglia.[47,55] It had revealed that complement C3/C3aR signaling is typically activated at the chronic stress, and C3aR blockade attenuated complement-mediated inflammatory pathway and synaptic pruning.[56] Here, we report that C3aR blockade could mimic the protective effect of NDRG2 overexpression on DACD. C3aR blockade improved the alternation triplet in Y maze and platform crossover in MWM test. C3aR blockade also rescued the reduction of total spine density and dendritic spine loss in diabetic mice. These results reflected the integrated molecular mechanism that abnormally high C3 levels act on C3aR to induce synaptic injury. However, it was rather challenging to obtain human hippocampal samples. Therefore, we used only mouse hippocampal samples to assess the molecular mechanism of diabetic cognitive dysfunction.

The incidence of dementia in diabetes in those who are younger than 60 is 0.5% per year.[57] The incidence then increases gradually (to 7%) in those over 60 years.[57] The hyperglycemia, microangiopathy, and macroangiopathy of diabetic patients contribute to executive dysfunction as well as mental and motor slowing.[58] C1q and C3 have been shown to be significantly increased in the brain tissue of AD patients,[28] and the expression levels of C3 in cerebrospinal fluid were significantly upregulated in AD patients.[59] RNA sequencing analysis of human hippocampus tissue has illustrated that C3/C3aR is closely associated with the diagnosis of dementia.[60] A previous clinical study showed that increased levels of C3 in the prefrontal cortex and serum of major depression patients.[61,62] Serum C3 is produced mainly by the liver.[63] Adipose tissue[64] and peripheral immune macrophages may also contribute to systemic C3 levels. Other studies showed that serum C3 is associated with insulin resistance and may reflect the progression of metabolic dysregulation, which eventually leads to abnormalities in glucose tolerance and T2DM.[65–68] Rasmussen et al. suggested that higher levels of serum C3 also increase the risk of diabetic retinopathy and neuropathy.[69] In addition, inhibition of serum C3 and fibrinogen interaction may be a potential novel therapeutic target to reduce diabetic cardiovascular disease[70] and thrombosis risk.[3,71]

Obtaining human cerebrospinal fluid is a challenging process. In this study, we collected the serum of 13 non-diabetic and 27 diabetic patients and evaluated cognitive function using DSST scores. We identified negative relationships between FPG & HOMA-IR and the cognitive function of diabetic patients, and DSST scores were negatively correlated with C3 levels in univariable logistic regression. However, risk factors, such as C3, FPG, and HOMA-IR value, were considered potential confounders in multivariate logistic regression analysis. Herein, we found that DSST score was only associated with groups and was significantly lower in diabetes than non-diabetes. We also acknowledged the limitation of small sample size in our study and expect to conduct multicenter and large-sample clinical studies to verify the potential risk factors, such as C3, FPG, or HOMA-IR value in DACD.

In conclusions, our study not only demonstrates the effectiveness and integrative mechanism of NDRG2 to improve cognitive function from a multi-omics perspective but also confirms the beneficial effects of NDRG2 from a micro perspective. The overexpression of astrocytic NDRG2 inhibits the over-activation of complement cascades mediated by C3 protein, thus alleviating cognitive dysfunction in diabetic mice. Our findings highlight the potential of NDRG2 targeting as an effective intervention to protect neuronal synapses in DACD.

Contributors

Qiang Wang, Yansong Li, and Tao Jiang designed this study. Qian Zhai, Chaoying Yan, and Zhi Ma contributed to the discussion. Tao Jiang, Kairui Pu, Meiyan Wu, and Mengyu Du performed the study. Shuxuan He, Mengyu Du, and Tao Jiang analyzed the results. Tao Jiang, Yansong Li, Ning Huang, and Qiang Wang wrote the manuscript. Tao Jiang and Yansong Li share the first authorship. Since Tao Jiang contributed more effort (in designing research studies, conducting experiments, and acquiring data) than Yansong Li, Tao Jiang was listed first. All authors read and approved the final version of the manuscript, and ensure it is the case.

Data sharing statement

Transcriptomic and proteomic sequencing data supporting our study findings are original and stored in CNSA (https://db.cngb.org/cnsa/) of CNGBdb (China National GeneBank DataBase) with accession number CNP0002799. http://db.cngb.org/cnsa/project/CNP0002799_a1910195/reviewlink/.

Declaration of interests

The authors declare no conflicts of interest.

Acknowledgements

We gratefully acknowledge engineer Ying Hao at the Instrumental Analysis Center of Xi'an Jiaotong University for technical assistance with the 3D structure reconstruction of dendritic spines.

Appendix A. Supplementary data

Supplementary data related to this article can be found at https://doi.org/10.1016/j.ebiom.2023.104653.

References

1 GBD 2017 Disease and Injury Incidence and Prevalence Collaborators. Global, regional, and national incidence, prevalence, and years lived with disability for 354 diseases and injuries for 195 countries and territories, 1990-2017: a systematic analysis for the Global Burden of Disease Study 2017. *Lancet*. 2018; 392(10159):1789–1858.
2 Zilliox LA, Chadrasekaran K, Kwan JY, Russell JW. Diabetes and cognitive impairment. *Curr Diab Rep*. 2016;16(9):87.
3 Gao Y, Xiao Y, Miao R, et al. The prevalence of mild cognitive impairment with type 2 diabetes mellitus among elderly people in China: a cross-sectional study. *Arch Gerontol Geriatr*. 2016;62:138–142.
4 Biessels GJ, Whitmer RA. Cognitive dysfunction in diabetes: how to implement emerging guidelines. *Diabetologia*. 2020;63(1):3–9.
5 Biessels GJ, Despa F. Cognitive decline and dementia in diabetes mellitus: mechanisms and clinical implications. *Nat Rev Endocrinol*. 2018;14(10):591–604.
6 Pearson-Stuttard J, Bennett J, Cheng YJ, et al. Trends in predominant causes of death in individuals with and without

diabetes in England from 2001 to 2018: an epidemiological analysis of linked primary care records. *Lancet Diabetes Endocrinol*. 2021;9(3):165–173.
7 Moon HY, Becke A, Berron D, et al. Running-induced systemic cathepsin B secretion is associated with memory function. *Cell Metab*. 2016;24(2):332–340.
8 Lourenco MV, Frozza RL, de Freitas GB, et al. Exercise-linked FNDC5/irisin rescues synaptic plasticity and memory defects in Alzheimer's models. *Nat Med*. 2019;25(1):165–175.
9 Yun SP, Kam TI, Panicker N, et al. Block of A1 astrocyte conversion by microglia is neuroprotective in models of Parkinson's disease. *Nat Med*. 2018;24(7):931–938.
10 Cheung G, Bataveljic D, Visser J, et al. Physiological synaptic activity and recognition memory require astroglial glutamine. *Nat Commun*. 2022;13(1):753.
11 Habib N, McCabe C, Medina S, et al. Disease-associated astrocytes in Alzheimer's disease and aging. *Nat Neurosci*. 2020;23(6):701–706.
12 Nation DA, Sweeney MD, Montagne A, et al. Blood-brain barrier breakdown is an early biomarker of human cognitive dysfunction. *Nat Med*. 2019;25(2):270–276.
13 Leardini-Tristao M, Andrade G, Garcia C, et al. Physical exercise promotes astrocyte coverage of microvessels in a model of chronic cerebral hypoperfusion. *J Neuroinflammation*. 2020;17(1):117.
14 Li Y, Yin A, Sun X, et al. Deficiency of tumor suppressor NDRG2 leads to attention deficit and hyperactive behavior. *J Clin Invest*. 2017;127(12):4270–4284.
15 Takarada-Iemata M, Yoshikawa A, Ta HM, et al. N-myc downstream-regulated gene 2 protects blood-brain barrier integrity following cerebral ischemia. *Glia*. 2018;66(7):1432–1446.
16 Hu XL, Liu XP, Deng YC, et al. Expression analysis of the NDRG2 gene in mouse embryonic and adult tissues. *Cell Tissue Res*. 2006;325(1):67–76.
17 Li X, Wu X, Luo P, Xiong L. Astrocyte-specific NDRG2 gene: functions in the brain and neurological diseases. *Cell Mol Life Sci*. 2020;77(13):2461–2472.
18 Skiriute D, Steponaitis G, Vaitkiene P, et al. Glioma malignancy-dependent NDRG2 gene methylation and downregulation correlates with poor patient outcome. *J Cancer*. 2014;5(6):446–456.
19 Yin A, Guo H, Tao L, et al. NDRG2 protects the brain from excitotoxicity by facilitating interstitial glutamate uptake. *Transl Stroke Res*. 2020;11(2):214–227.
20 Guo H, Yin A, Ma Y, et al. Astroglial N-myc downstream-regulated gene 2 protects the brain from cerebral edema induced by stroke. *Glia*. 2021;69(2):281–295.
21 Tao L, Zhu Y, Wang R, et al. N-myc downstream-regulated gene 2 deficiency aggravates memory impairment in Alzheimer's disease. *Behav Brain Res*. 2020;379:112384.
22 Ichikawa T, Nakahata S, Tamura T, Manachai N, Morishita K. The loss of NDRG2 expression improves depressive behavior through increased phosphorylation of GSK3beta. *Cell Signal*. 2015;27(10):2087–2098.
23 Stogsdill JA, Ramirez J, Liu D, et al. Astrocytic neuroligins control astrocyte morphogenesis and synaptogenesis. *Nature*. 2017;551(7679):192–197.
24 Nagai J, Rajbhandari AK, Gangwani MR, et al. Hyperactivity with disrupted attention by activation of an astrocyte synaptogenic cue. *Cell*. 2019;177(5):1280–1292.e20.
25 Chung WS, Allen NJ, Eroglu C. Astrocytes control synapse formation, function, and elimination. *Cold Spring Harb Perspect Biol*. 2015;7(9):a020370.
26 Santello M, Toni N, Volterra A. Astrocyte function from information processing to cognition and cognitive impairment. *Nat Neurosci*. 2019;22(2):154–166.
27 Adamsky A, Kol A, Kreisel T, et al. Astrocytic activation generates de novo neuronal potentiation and memory enhancement. *Cell*. 2018;174(1):59–71.e14.
28 Liddelow SA, Guttenplan KA, Clarke LE, et al. Neurotoxic reactive astrocytes are induced by activated microglia. *Nature*. 2017;541(7638):481–487.
29 Lian H, Yang L, Cole A, et al. NFkappaB-activated astroglial release of complement C3 compromises neuronal morphology and function associated with Alzheimer's disease. *Neuron*. 2015;85(1):101–115.
30 Schartz ND, Tenner AJ. The good, the bad, and the opportunities of the complement system in neurodegenerative disease. *J Neuroinflammation*. 2020;17(1):354.
31 King BC, Blom AM. Complement in metabolic disease: meta-flammation and a two-edged sword. *Semin Immunopathol*. 2021;43(6):829–841.
32 Stokowska A, Atkins AL, Moran J, et al. Complement peptide C3a stimulates neural plasticity after experimental brain ischaemia. *Brain*. 2017;140(2):353–369.
33 Joshi AU, Minhas PS, Liddelow SA, et al. Fragmented mitochondria released from microglia trigger A1 astrocytic response and propagate inflammatory neurodegeneration. *Nat Neurosci*. 2019;22(10):1635–1648.
34 Moien-Afshari F, Ghosh S, Elmi S, et al. Exercise restores endothelial function independently of weight loss or hyperglycaemic status in db/db mice. *Diabetologia*. 2008;51(7):1327–1337.
35 Lee JH, Kim JY, Noh S, et al. Astrocytes phagocytose adult hippocampal synapses for circuit homeostasis. *Nature*. 2021;590(7847):612–617.
36 Swarup V, Chang TS, Duong DM, et al. Identification of conserved proteomic networks in neurodegenerative dementia. *Cell Rep*. 2020;31(12):107807.
37 Wisniewski JR, Zougman A, Nagaraj N, Mann M. Universal sample preparation method for proteome analysis. *Nat Methods*. 2009;6(5):359–362.
38 Zhu Y, Xu H, Chen H, et al. Proteomic analysis of solid pseudopapillary tumor of the pancreas reveals dysfunction of the endoplasmic reticulum protein processing pathway. *Mol Cell Proteomics*. 2014;13(10):2593–2603.
39 Di Liberto G, Pantelyushin S, Kreutzfeldt M, et al. Neurons under T Cell attack coordinate phagocyte-mediated synaptic stripping. *Cell*. 2018;175(2):458–471.e19.
40 Owen B, Bichler E, Benveniste M. Excitatory synaptic transmission in hippocampal area CA1 is enhanced then reduced as chronic epilepsy progresses. *Neurobiol Dis*. 2021;154:105343.
41 Leinenga G, Gotz J. Scanning ultrasound removes amyloid-beta and restores memory in an Alzheimer's disease mouse model. *Sci Transl Med*. 2015;7(278):278ra33.
42 Ye T, Meng X, Wang R, et al. Gastrodin alleviates cognitive dysfunction and depressive-like behaviors by inhibiting ER stress and NLRP3 inflammasome activation in db/db mice. *Int J Mol Sci*. 2018;19(12):3977.
43 Liu Z, Dai X, Zhang H, et al. Gut microbiota mediates intermittent-fasting alleviation of diabetes-induced cognitive impairment. *Nat Commun*. 2020;11(1):855.
44 Horowitz AM, Fan X, Bieri G, et al. Blood factors transfer beneficial effects of exercise on neurogenesis and cognition to the aged brain. *Science*. 2020;369(6500):167–173.
45 Johnson ECB, Dammer EB, Duong DM, et al. Large-scale proteomic analysis of Alzheimer's disease brain and cerebrospinal fluid reveals early changes in energy metabolism associated with microglia and astrocyte activation. *Nat Med*. 2020;26(5):769–780.
46 Vasek MJ, Garber C, Dorsey D, et al. A complement-microglial axis drives synapse loss during virus-induced memory impairment. *Nature*. 2016;534(7608):538–543.
47 Propson NE, Gedam M, Zheng H. Complement in neurologic disease. *Annu Rev Pathol*. 2021;16:277–298.
48 Xin W, Chan JR. That wasn't a complement-too much C3 in demyelinating disease. *Immunity*. 2020;52(1):11–13.
49 Zhao Y, Luo C, Chen J, et al. High glucose-induced complement component 3 up-regulation via RAGE-p38MAPK-NF-kappaB signalling in astrocytes: in vivo and in vitro studies. *J Cell Mol Med*. 2018;22(12):6087–6098.
50 Flugge G, Araya-Callis C, Garea-Rodriguez E, Stadelmann-Nessler C, Fuchs E. NDRG2 as a marker protein for brain astrocytes. *Cell Tissue Res*. 2014;357(1):31–41.
51 Zhang Z, Ma Z, Zou W, et al. N-myc downstream-regulated gene 2 controls astrocyte morphology via Rho-GTPase signaling. *J Cell Physiol*. 2019;234(11):20847–20858.
52 Zahir F, Firth HV, Baross A, et al. Novel deletions of 14q11.2 associated with developmental delay, cognitive impairment and similar minor anomalies in three children. *J Med Genet*. 2007;44(9):556–561.
53 Lee A, Lim S, Oh J, et al. NDRG2 expression in breast cancer cells downregulates PD-L1 expression and restores T cell proliferation in tumor-coculture. *Cancers (Basel)*. 2021;13(23):6112.
54 Lee KW, Lim S, Kim KD. The function of N-myc downstream-regulated gene 2 (NDRG2) as a negative regulator in tumor cell metastasis. *Int J Mol Sci*. 2022;23(16):9365.
55 Wei Y, Chen T, Bosco DB, et al. The complement C3-C3aR pathway mediates microglia-astrocyte interaction following status epilepticus. *Glia*. 2021;69(5):1155–1169.

56 Zhang MM, Guo MX, Zhang QP, et al. IL-1R/C3aR signaling regulates synaptic pruning in the prefrontal cortex of depression. *Cell Biosci*. 2022;12(1):90.
57 Exalto LG, Biessels GJ, Karter AJ, et al. Risk score for prediction of 10 year dementia risk in individuals with type 2 diabetes: a cohort study. *Lancet Diabetes Endocrinol*. 2013;1(3):183–190.
58 McCrimmon RJ, Ryan CM, Frier BM. Diabetes and cognitive dysfunction. *Lancet*. 2012;379(9833):2291–2299.
59 Wu T, Dejanovic B, Gandham VD, et al. Complement C3 is activated in human AD brain and is required for neurodegeneration in mouse models of amyloidosis and tauopathy. *Cell Rep*. 2019;28(8):2111–21123.e6.
60 Litvinchuk A, Wan YW, Swartzlander DB, et al. Complement C3aR inactivation attenuates tau pathology and reverses an immune network deregulated in tauopathy models and Alzheimer's disease. *Neuron*. 2018;100(6):1337–13353.e5.
61 Crider A, Feng T, Pandya CD, et al. Complement component 3a receptor deficiency attenuates chronic stress-induced monocyte infiltration and depressive-like behavior. *Brain Behav Immun*. 2018;70:246–256.
62 Yang X, Tao H, Xiao L, Li C, Tang Y, Liu Y. Increased serum C3 and decreased UA in patients of bipolar disorder in Chinese han population. *Front Psychiatry*. 2018;9:381.
63 Alper CA, Johnson AM, Birtch AG, Moore FD. Human C'3: evidence for the liver as the primary site of synthesis. *Science*. 1969;163(3864):286–288.
64 Choy LN, Rosen BS, Spiegelman BM. Adipsin and an endogenous pathway of complement from adipose cells. *J Biol Chem*. 1992;267(18):12736–12741.
65 Wlazlo N, van Greevenbroek MM, Ferreira I, et al. Complement factor 3 is associated with insulin resistance and with incident type 2 diabetes over a 7-year follow-up period: the CODAM Study. *Diabetes Care*. 2014;37(7):1900–1909.
66 Somani R, Richardson VR, Standeven KF, Grant PJ, Carter AM. Elevated properdin and enhanced complement activation in first-degree relatives of South Asian subjects with type 2 diabetes. *Diabetes Care*. 2012;35(4):894–899.
67 Muscari A, Antonelli S, Bianchi G, et al. Serum C3 is a stronger inflammatory marker of insulin resistance than C-reactive protein, leukocyte count, and erythrocyte sedimentation rate: comparison study in an elderly population. *Diabetes Care*. 2007;30(9):2362–2368.
68 Weyer C, Tataranni PA, Pratley RE. Insulin action and insulinemia are closely related to the fasting complement C3, but not acylation stimulating protein concentration. *Diabetes Care*. 2000;23(6):779–785.
69 Rasmussen KL, Nordestgaard BG, Nielsen SF. Complement C3 and risk of diabetic microvascular disease: a cohort study of 95202 individuals from the general population. *Clin Chem*. 2018;64(7):1113–1124.
70 King R, Tiede C, Simmons K, Fishwick C, Tomlinson D, Ajjan R. Inhibition of complement C3 and fibrinogen interaction: a potential novel therapeutic target to reduce cardiovascular disease in diabetes. *Lancet*. 2015;385(Suppl 1):S57.
71 King RJ, Schuett K, Tiede C, et al. Fibrinogen interaction with complement C3: a potential therapeutic target to reduce thrombosis risk. *Haematologica*. 2021;106(6):1616–1623.